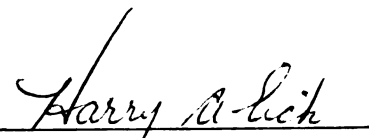


THE VAPORIZATION THERMODYNAMICS
OF SAMARIUM DICARBIDE AND
THULIUM DICARBIDE

Thesis for the Degree of Ph. D.
MICHIGAN STATE UNIVERSITY
ROBERT LANE SEIVER
1971



This is to certify that the
 thesis entitled
 The Vaporization Thermodynamics
 of Samarium Dicarbide and
 Thulium Dicarbide
 presented by
 Robert Lane Seiver
 has been accepted towards fulfillment
 of the requirements for
Ph.D. degree in Chemistry


 Major professor

Date August 12, 1971

Q-7639



6-11-11

1

ABSTRACT

THE VAPORIZATION THERMODYNAMICS OF SAMARIUM DICARBIDE AND THULIUM DICARBIDE

By

Robert Lane Seiver

Several investigations of the vaporization of SmC_2 have been reported. The reported values of the equilibrium decomposition pressures are in only fair agreement and some workers report a variation in the enthalpy of decomposition of SmC_2 with the amount of free carbon present. The present study was undertaken to examine this apparent composition dependence and to study the previously unreported vaporization of TmC_2 .

The dicarbides were prepared by direct combination of the elements under argon in sealed tantalum ampoules. Chemical analysis indicated that the products were generally metal-rich, $1.78 \leq \text{C/M} \leq 2.02$. X-Ray powder diffraction patterns showed only the body centered tetragonal CaC_2 -type structure for SmC_2 preparations and those TmC_2 preparations which were cooled quickly. Preparations of TmC_2 which were cooled slowly yielded the black low-symmetry modification previously reported. Preliminary single-crystal X-ray diffraction data indicate that this modification is actually a mixture of a hexagonal phase, $\underline{a} = 3.19 \pm 0.01 \text{ \AA}$, $\underline{c} = 16.74 \pm 0.07 \text{ \AA}$; and an orthorhombic phase, $\underline{a} = 3.68 \pm 0.01 \text{ \AA}$, $\underline{b} = 12.40 \pm 0.04 \text{ \AA}$, and $\underline{c} = 13.58 \pm 0.03 \text{ \AA}$. The

mixture quickly reverted to the tetragonal structure on heating in vacuum.

Mass spectrometric observation of the effusate of TmC_2 vaporization with a 30 or 55 ev ionizing electron beam showed only Tm^+ . Its appearance potential was 5.7 ev. Limits were set for carbide vapor species at $I_{\text{TmC}_2^+} < 0.005 I_{\text{Tm}^+}$ and $I_{\text{TmC}^+} < 0.02 I_{\text{Tm}^+}$.

Vapor pressure measurements were made by target collection Knudsen effusion. The effusate was condensed onto chilled aluminum targets which were analyzed quantitatively by X-ray fluorescence. Metal-rich samples of SmC_2 or TmC_2 initially showed high erratic pressures. Calculations from weight loss data indicated that stable pressures were achieved very close to the $\text{MC}_{2.00}$ composition.

Carbon-rich samples ($3 < \text{C/M} < 12$) showed the lower enthalpy previously reported, but this was found to be a time-dependent behavior. After several hours of heating the vapor pressures returned to the values measured over near-stoichiometric samples. It was determined that this initial behavior was due to oxygen contamination which results from hydrolysis by atmospheric water vapor. The oxide species are reduced by the excess carbon, releasing free metal.

Vapor pressures over SmC_2 measured when oxygen contamination was absent were in good agreement with those reported by two earlier workers who used methods unlikely to be seriously affected by oxygen contamination. The data from the three studies were combined to give for the pressure of Sm(g) over $\text{SmC}_2(\text{s})$,

$$\ln P_{\text{Sm}}(\text{atm}) = [(-31,520 \pm 300)/T] + (8.15 \pm 0.20) \quad (1)$$

over the temperature range 1400–2080 K.

Vapor pressures of Tm(g) over $\text{TmC}_2\text{(s)}$ measured when oxygen contamination was absent were fitted to the line

$$\ln P_{\text{Tm}}(\text{atm}) = [(-35,570 \pm 340)/T] + (8.98 \pm 0.18) \quad (2)$$

over the temperature range 1660–2130 K.

Second law data reduction, carried out using heat capacities estimated from that of CaC_2 , gave $\Delta H_{\text{V}298}^\circ(\text{SmC}_2) = 66.9 \pm 1.0$ kcal/gfw, $\Delta S_{\text{V}298}^\circ(\text{SmC}_2) = 21.4 \pm 1.0$ eu; $\Delta H_{\text{V}298}^\circ(\text{TmC}_2) = 79.1 \pm 1.3$ kcal/gfw, $\Delta S_{\text{V}298}^\circ(\text{TmC}_2) = 27.5 \pm 1.3$ eu. Third law calculations were made using the standard entropy of CaC_2 and Latimer's method; it was necessary to employ a non-degenerate ground electronic state for Tm^{+3} in TmC_2 . This is in accord with the observation that TmC_2 does not undergo an antiferromagnetic transition at low temperatures. Results of the third law calculations were $\Delta H_{\text{V}298}^\circ(\text{SmC}_2) = 66.5 \pm 3.0$ kcal/gfw, $\Delta H_{\text{V}298}^\circ(\text{TmC}_2) = 78.7 \pm 3.0$ kcal/gfw.

Thermodynamic calculations involving the reduction of sesquioxide by graphite indicate that the proposed effect of oxide contamination is feasible for SmC_2 and TmC_2 . They further indicate that oxide contamination might interfere in the vaporization of HoC_2 and EuC_2 , but not in that of any other lanthanide dicarbide.

For $\text{SmC}_2\text{(s)}$ and $\text{TmC}_2\text{(s)}$, respectively, $\Delta H_{\text{f}298}^\circ$ are -17.5 ± 1.3 and -23.6 ± 2.0 kcal/gfw.

THE VAPORIZATION THERMODYNAMICS OF
SAMARIUM DICARBIDE AND THULIUM DICARBIDE

By

Robert Lane Seiver

A THESIS

Submitted to

Michigan State University

in partial fulfillment of the requirements

for the degree of

DOCTOR OF PHILOSOPHY

Department of Chemistry

1971

ACKNOWLEDGEMENTS

The author wishes to express his sincere gratitude to Professor Harry A. Eick for his guidance, encouragement, and assistance throughout the past four years.

A heartfelt thank you is also extended to my wife, Barbara-Kay. Without her enthusiasm and support the attainment of this educational goal would not have been possible, and without her assistance in typing this manuscript it would have been much more difficult.

The past and present members of the High Temperature Group have contributed to this work both by direct suggestions and by their general attitude of professionalism and intellectual curiosity. Their assistance is greatly appreciated.

A special expression of thanks is extended to Dr. Norman Stout for his thorough critical review of the work on which this thesis is based.

The financial support of the Atomic Energy Commission under contract AT (11-1)-716 and of the National Aeronautics and Space Administration is gratefully acknowledged.

TABLE OF CONTENTS

	Page
I. Introduction	1
II. Previous Investigations of the Lanthanide Dicarbides	3
A. Preparative Investigations	3
B. Structural Investigations	3
C. Thermochemical Investigations	4
1. Vaporization Thermodynamics	4
2. Formation of Gaseous Molecules	6
3. Calorimetric Measurements	6
D. Other Investigations	6
E. Other Relevant Dicarbides	7
III. Theoretical Considerations Pertinent to This Investigation	8
A. Phase Relationships and Thermodynamic Behavior	8
1. The Phase Rule	8
2. The Thermodynamics of Equilibrium	9
B. Physical Methods of Measurement	9
1. Vapor Pressure Measurements	9
2. Theory of Knudsen Effusion	10
3. The Target Collection Method	11
4. Theoretical Limitations of the Knudsen Method	11
a. The Non-Ideal Orifice	11
b. The Steady State Approximation	12
c. Viscous Flow	12

TABLE OF CONTENTS (Cont.)	Page
d. Small Knudsen Cells	13
e. Vaporization Coefficient	13
f. Surface Diffusion	14
5. Practical Limitations of the Knudsen Method	14
a. Characterization of Condensed Phases	14
b. Diffusion-Limited Vaporization	14
c. Container Losses	15
d. Collection Losses	15
e. Other Limitations	16
6. Temperature Measurement	16
7. X-Ray Fluorescence Analysis	17
C. Thermodynamic Data Reduction	17
1. Second Law Calculations	17
2. Third Law Calculations	18
3. Derived Thermodynamic Quantities	19
IV. Experimental Methods	21
A. Materials	21
B. Preparation	21
C. Sample Handling	22
D. Chemical Analysis	22
1. Free Carbon Analysis	22
2. Thulium and Samarium Analysis	23
3. Total Carbon Analysis	23
4. Oxygen Analysis	23
E. X-Ray Diffraction	24
F. Mass Spectrometry	24
G. Target Collection Techniques	24

TABLE OF CONTENTS (Cont.)	Page
H. X-Ray Fluorescence Analysis	25
1. Spectrometer Operation	25
2. Spectrometer Calibration	25
I. Temperature Measuring Equipment	26
J. Specific Experimental Conditions	26
V. Results	28
A. Preparative	28
B. Analytical	28
1. Chemical Analysis	28
2. X-Ray Powder Diffraction Analysis	29
C. Mass Spectrometry Results	30
1. Vaporization Mode	30
2. Appearance Potential	30
D. Vaporization Results	31
1. Behavior of Metal-Rich Samples	31
2. Behavior of Carbon-Rich Samples	31
3. Container Interaction	34
4. Evidence of Contaminant Interaction	34
5. Confirmation of Contaminant Interaction	35
6. Vapor Pressure Equations for SmC_2	36
7. Vapor Pressure Equation for TmC_2	38
E. Thermodynamic Data Reduction	38
1. Thermodynamic Values Employed	38
a. Heat Capacity Functions	38
b. Absolute Entropies	40
c. Free Energy Functions	40
d. Additional Thermochemical Values	40

TABLE OF CONTENTS (Cont.)	Page
2. Results of Second Law Treatment	41
3. Results of Third Law Treatment	41
4. The Absolute Entropy of Thulium Dicarbide	42
F. Thermodynamic Treatment of the Contaminant Reaction	44
1. The Reactions Involved	44
2. A Kinetically Controlled Vaporization	44
3. The Phase Rule	45
4. Results	45
5. Extension to Other Lanthanide Dicarbides	47
VI. Discussion	52
A. Evaluation of Experimental Conditions	52
1. Sample Handling	52
2. The Attainment of Knudsen Conditions	52
3. An Improved Target Collection Apparatus	53
4. Fluorescence Analysis	54
5. Temperature Measurement	55
B. The Effects of Oxide Contamination	55
1. Explanation of the Anomalous Behavior	55
2. The Kinetics Involved	56
3. The Reaction Trend	57
4. Observations Concerning the Preparation of YbC_2 and EuC_2	57
C. Evaluation of Thermochemical Results	57
1. Comparison with Previous Work	57
2. The Low Temperature Modification of TmC_2	58
3. Validity of the Thermodynamic Approximations	58

TABLE OF CONTENTS (Cont.)	Page
D. The Electronic Ground State of TmC_2	59
E. The Correlation in Vaporization of the Lanthanide and Alkaline Earth Metals and Their Dicarbides	60
VII. Suggestions for Future Research	62
REFERENCES	64
APPENDICES	72

LIST OF TABLES

TABLE		Page
1.	Results of Previous Vapor Pressure Measurements in the Samarium-Carbon System	5
2.	Observed Lattice Parameters of Phases Prepared in This Study	30
3.	Summary of Thermodynamic Results	43

LIST OF FIGURES

FIGURE	Page
1. Ionization Efficiency Curves	32
2. Vaporization Behavior of Carbon-Rich Samples	33
3. Equilibrium Pressure of Samarium Vapor Over Samarium Dicarbide	37
4. Equilibrium Pressure of Thulium Vapor Over Thulium Dicarbide	39
5. Equilibrium Samarium Pressure Reported for SmC_2 and Calculated for $\text{Sm}_2\text{O}_3\text{-C}$	46
6. Equilibrium Thulium Pressure Reported for TmC_2 and Calculated for $\text{Tm}_2\text{O}_3\text{-C}$	48
7. Equilibrium Ytterbium Pressure Reported for YbC_2 and Calculated for $\text{Yb}_2\text{O}_3\text{-C}$	49
8. Equilibrium Europium Pressure Reported for EuC_2 and Calculated for $\text{Eu}_2\text{O}_3\text{-C}$	51
9. The Correlation of the Metal and Metal Dicarbide Vaporizations	61
A-1. Parts of the Guinier Camera	81

LIST OF APPENDICES

APPENDIX	Page
I. Instructions for Realigining the Guinier Cameras	73
II. The Observed Powder Diffraction Pattern of the Black Form of TmC_2	82
III. Values of Δf_{ef} For Reactions (V-1) and (V-2)	84
IV. Equilibrium Pressure and Third Law Enthalpy Data	85
IVA. Samarium Dicarbide	85
IVB. Thulium Dicarbide	87

CHAPTER I

INTRODUCTION

The urge to classify and to identify trends has been at once the salvation and perdition of the modern chemist. The sheer bulk of data available must be systematized to be comprehensible, and indeed the "scientific method" involves extrapolating trends or hypotheses to suggest new experiments. Yet not all the experiments can be carried out, and all too often the trend is accepted as data rather than extrapolation, and new information is buried by the very process intended to dig it out.

The overall similarity of the lanthanide elements makes their chemistry a prime target for classification. The ability to vary constituent properties slowly and continuously is a powerful tool which has given inorganic chemists more sophisticated models of chemical behavior than would have otherwise been possible. At the same time it has led to the unfortunate practice of extrapolating for the properties of the less common and less well-behaved lanthanides.

The present study illustrates the full spectrum of the benefits and hazards of classification. It has succeeded in its original goal of extending a correlation between the enthalpy of vaporization of the lanthanide dicarbides and the vapor pressures of the respective metals, and of investigating an apparent anomaly in that correlation. It has also revealed conditions where the smooth progression of lanthanide properties results in a complete reversal of the preferred reaction path. It has pointed out an instance where the reaction path cannot be

predicted from this trend because of insufficient auxiliary data. And finally, it has given an instance where a widely accepted correlation, namely, that crystal field splittings of the lanthanides are chemically insignificant, may be invalid.

CHAPTER II

PREVIOUS INVESTIGATIONS OF THE LANTHANIDE DICARBIDES

The general topic of metal carbides was reviewed thoroughly in a recent article by Frad¹. The literature through 1967 was examined extensively and the review is recommended as a concise compilation of the then available information on preparation, structure and thermochemistry.

A. Preparative Investigations

Moissan² reported preparing a rare earth carbide by reducing the oxide with graphite, and von Stackelberg³ prepared dicarbides of several lanthanides. The first systematic preparation and characterization of the dicarbides of the lanthanides (except europium and promethium) was reported by Spedding et al.⁴, who combined the elements directly. Vickery et al.⁵ showed that these same dicarbide phases could be prepared by Moissan's method, and that formation proceeded via the metal. Europium dicarbide was more difficult to prepare⁶ and was finally reported by Gebelt and Eick⁷. To date no carbides have been reported for promethium, a synthetic radioactive element.

B. Structural Investigations

Von Stackelberg³ reported X-ray powder diffraction data on the room-temperature modification of the dicarbides which showed them to be body-centered tetragonal, isostructural with CaC_2 . At high temperature they

convert to a cubic structure⁸ which for some mixed-lanthanide dicarbides⁹ is stable at room temperature. The cubic-tetragonal transformation temperatures and MC_2 -C eutectic temperatures have been reported¹⁰. Extensive neutron-diffraction studies by Atoji¹¹⁻¹⁶ show one or more antiferromagnetic transitions at low temperature for most of the dicarbides, but none for TmC_2 ¹⁷ and only a poorly defined change for YbC_2 ¹⁸.

Krupka et al.¹⁹ reported that another form of the dicarbide could be prepared for the heavy lanthanides (Tb, Dy, Ho, Er, Tm, Yb, Lu, Y) by annealing under pressure. This form gave a very complex X-ray powder diffraction pattern which was tentatively indexed on an orthorhombic unit cell.

C. Thermochemical Investigations

1. Vaporization Thermodynamics

Due to the refractory nature of these compounds most thermochemical studies have been done by high-temperature vaporization methods. Thermochemical values for thermal decomposition of the dicarbide have been reported for La^{20,21}, Ce²¹⁻²³, Nd²¹, Sm^{21,24-29}, Eu^{21,24,30}, Gd^{31,32}, Dy^{33,34}, Ho³³⁻³⁵, Er³⁶, and Yb³⁷. Haschke³⁷ has shown that the enthalpy of vaporization is correlated to the vapor pressure of the corresponding metal.

Several investigations of the vaporization of SmC_2 have been reported. However, the reported values of the equilibrium decomposition pressures are in only fair agreement, and, as is shown in Table 1, some investigators report a variation in the enthalpy of decomposition of SmC_2 with the amount of free carbon present.

The X-ray data reported by the Russian workers²⁸⁻²⁹ show that their samples were grossly contaminated and their work can be discounted.

Table 1

Results of Previous Vapor Pressure Measurements in the Samarium-Carbon System

Reference	Author	Method	C/Sm	ΔH°_T , kcal/gfw	ΔS°_T , eu
24	Cuthbert, <u>et al.</u>	Target coll.	2.0-2.3	61.5 ± 1.2	15.5 ± 0.7
		Mass spec.	2.0-2.1	78.2 ± 2.3	27.6 ± 1.8
		Mass spec.	2.1-9	66.4 ± 1.7	19.0 ± 1.4
25	Avery, <u>et al.</u>	Mass spec.	2.0-2.1	76.9 ± 1.7	27.0 ± 1.4
		Mass spec.	2.1-23	65.2 ± 0.4	18.7 ± 0.3
21	Faircloth, <u>et al.</u>	Target coll.	2.0-3.1	63.3 ± 0.8	16.5 ± 0.4
27	Stout, <u>et al.</u>	Torsion effusion	2.0-2.8	61.6	16.0
26	Pilato	Mass spec.	C liner	58.6 ± 2.1	13.7 ± 1.8

Reasons for disagreement among the other workers are not so apparent.

No study of the decomposition pressure of thulium dicarbide has been reported.

2. Formation of Gaseous Molecules

The dicarbides of the less volatile lanthanides vaporize by two modes, giving both gaseous metal atoms and carbide molecules. Both the dicarbide and tetracarbide have been observed. The equilibria of these molecules with the gaseous metals are pressure-independent reactions and can be studied by mass spectrometry without extensive calibration. Dissociation and atomization energies have been reported for the gaseous carbides of La^{38,39}, Ce^{22,39-41}, Pr^{39,40}, Nd^{39,41-43}, Gd⁴⁴, Tb⁴⁴, Dy^{33,34}, Ho^{33,34,40}, and Er³⁶. Gaseous molecules have been found to be absent in the vaporization of SmC₂^{24-26,45}, EuC₂^{24,45}, and YbC₂³⁷.

3. Calorimetric Measurements

Baker et al.⁴⁶ measured the enthalpy of formation of CeC₂ by oxygen bomb calorimetry and got results in reasonable agreement with those from vaporization studies. No heat capacity measurement has been reported.

D. Other Investigations

The dicarbides are considered to be ionic salts of acetylide, C²⁻, with the metals, which are usually trivalent. Considerable interest arose concerning the character of the third electron. Magnetic measurements^{47,48} and X-ray absorption edge studies⁴⁹ showed that the metals are indeed trivalent and the extra electron is delocalized in a conduction band. Neutron diffraction work¹¹⁻¹⁸ confirms this conclusion for the commonly trivalent metals and gives an oxidation state of +2.7 for Yb in YbC₂. Neutron diffraction data for EuC₂ and SmC₂ are not yet available.

Hydrolysis studies of the lanthanide dicarbides under controlled conditions have been reported^{50,51}.

E. Other Relevant Dicarbides

Since no heat capacity data have been reported for the lanthanide dicarbides, it is necessary to estimate thermal functions to reduce thermochemical data to standard conditions for comparison purposes. The isostructural compound CaC_2 has usually been chosen as a basis for such estimates. Its standard entropy⁵², high temperature heat capacity⁵³, and enthalpy of the tetragonal to cubic transformation have been compiled by Wicks and Block⁵⁴.

A more reliable standard entropy is available for thorium dicarbide⁵⁵ and its high-temperature heat capacity has been estimated⁵⁶ by use of Krikorian's method⁵⁷, but ThC_2 is not isostructural⁵⁸ with the lanthanide dicarbides.

Uranium dicarbide is isostructural^{59,60} with CaC_2 and LnC_2 , and its low temperature^{61,62} and high temperature⁶³⁻⁶⁵ heat capacities have been measured. However, this compound is metastable and significantly substoichiometric ($\text{C/U} = 1.91\text{--}1.93$) and not as suitable a basis for estimation.

CHAPTER III

THEORETICAL CONSIDERATIONS PERTINENT TO THIS INVESTIGATION

A. Phase Relationships and Thermodynamic Behavior

1. The Phase Rule

Conditions necessary for equilibrium in a vaporization study are given⁶⁶ by Gibb's phase rule (III-1). The number of degrees of freedom,

$$F = C - P + 2 \qquad \text{III-1}$$

F, is expressed in terms of the number of components, C, and the number of phases, P. Number of components is defined as the smallest number of independently variable constituents needed to define the system. Two general categories describe most vaporization processes in terms of this rule.

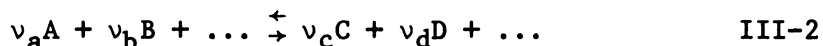
In the first, congruent vaporization, the composition of the vapor is the same as that of the single condensed phase. This composition restriction makes it possible to define the system with only one component, and since there are two phases, $F = 1$. Fixing the temperature removes all degrees of freedom and fixes the pressure.

Incongruent vaporization of a condensed phase gives a second condensed phase and a vapor of different composition. Here there are three constituents, but because of the chemical reaction relating them the system may be defined with two components. There are three phases, so again the system is univariant and fixing the temperature defines the pressure.

Systems involving condensed phases of variable composition or vapors with more than one constituent require a more detailed analysis.

2. The Thermodynamics of Equilibrium

Under conditions of constant temperature and pressure, the thermodynamic statement of equilibrium for the general reaction (III-2) is $\Delta G = 0$.



Substituting into the mass action equation (III-3)⁶⁷ and noting that

$$\Delta G_T = \Delta G_T^\circ + RT \ln \frac{(a_C)^{\nu_c} (a_D)^{\nu_d} \dots}{(a_A)^{\nu_a} (a_B)^{\nu_b} \dots} \quad \text{III-3}$$

at equilibrium the mass action coefficient is the equilibrium constant gives equation (III-4). Normally in effusion studies the condensed phases

$$\Delta G_T^\circ = -RT \ln K_T \quad \text{III-4}$$

are considered to be present in pure form, at unit activity, and the vapor consists of a single species. Since the vapor is dilute enough to be considered ideal, equation (III-5) results. Thus measurement of the vapor

$$\Delta G_T^\circ = -RT \ln P_T \quad \text{III-5}$$

pressure at a series of temperatures yields the standard free energy change and its temperature dependence, from which a variety of thermodynamic functions may be calculated as described in section III,C.

B. Physical Methods of Measurement

1. Vapor Pressure Measurements

The compounds studied are quite refractory, with vapor pressures of 10^{-9} to 10^{-3} atm in a conveniently attainable temperature range. Such pressures may be measured⁶⁸ by either Langmuir free evaporation or Knudsen effusion methods. The method chosen for this study was Knudsen effusion, which is based on the rate of effusion of the vapor through an orifice into vacuum. Determination of this rate may involve microbalance, torsion,

target collection, or mass spectrometric measurements, or some combination of these. Mass spectrometry gives information regarding the nature of the gaseous species, but a spectrometer is difficult to calibrate for absolute pressures. Spectrometry was used to identify the effusate vapor and the target collection procedure was employed in the vapor pressure measurements.

2. Theory of Knudsen Effusion

The theoretical treatment of molecular effusion was first described by Knudsen^{69,70} and more recently in a general review by Cater⁶⁸ and in more detail by Ward⁷¹. The derivation is based on the kinetic theory of dilute gases and in particular on the Maxwell-Boltzmann distribution of molecular velocities in such a gas. From this distribution it can be shown that the number of molecules which pass through an infinitesimal plane area δS from one side to the other in time interval δt is given by equation (III-6), where n is the

$$N = \frac{n\bar{v}}{4} \delta S \delta t \quad \text{III-6}$$

density, molecules per unit volume, and \bar{v} is the average speed. If δS is a portion of the container wall, inclusion of the momentum transfer per collision gives the kinetic theory derivation for the vapor pressure. Alternatively, if δS is an orifice in that (infinitesimally thin) wall, equation (III-6) gives the rate of effusion through the orifice. For a finite orifice, S_o , and time interval, t , provided that the loss of molecules through the orifice does not significantly alter the equilibrium or velocity distribution, the effusion rate is given by equation (III-7). This equation may be

$$N = \frac{n\bar{v}S_o t}{4} \quad \text{III-7}$$

combined with $\bar{v} = (8RT/\pi M)^{1/2}$ from kinetic theory and with the ideal gas law to give equation (III-8) in which W is the mass of the effusate.

$$P = \left(\frac{W}{S_0 t} \right) \left(\frac{2\pi RT}{M} \right)^{1/2} \quad \text{III-8}$$

3. The Target Collection Method

The rate of effusion can be determined by collecting and analyzing a known fraction of the effusate. To determine the fraction collected it is necessary to know the angular distribution of the effusing molecules. The fraction of molecules from an ideal orifice passing through the solid angle increment $d\omega$ is given by the cosine rule, (III-9).

$$\frac{dN}{N} = \pi^{-1} \cos \theta \, d\omega \quad \text{III-9}$$

Here θ is the angle between the normal to the orifice and the axis of $d\omega$. Integration over the solid angle subtended by a circular collector of radius r , coaxial with the orifice and at distance d from it, gives for the fraction collected $r^2/(d^2+r^2)$. This factor is combined with equation (III-8) to give (III-10) where W now refers to the mass of the

$$P = \frac{3.760 \times 10^{-4} W}{S_0 t} \left(\frac{T}{M} \right)^{1/2} \left(\frac{d^2 + r^2}{r^2} \right) \quad \text{III-10}$$

fraction of effusate which strikes the target. Dimensions are P in atm, S_0 in cm^2 , t in min, and W in g.

4. Theoretical Limitations of the Knudsen Method

a. The Non-Ideal Orifice

In practice the orifice cannot be located in an infinitesimally thin wall, but is instead a channel of some finite length. Molecules which enter the orifice and strike the wall of the channel are re-emitted according to the cosine rule, and may be returned to the inside of the cell. The calculation of the decrease from the ideal effusion rate was first carried out by Clausing⁷² for channel

orifices and the correction term is called the Clausing factor. A conical orifice behaves more nearly ideally, especially at small values of θ . Effusion probabilities for conical orifice geometry have been evaluated by Freeman and Edwards⁷³.

b. The Steady State Approximation

The derivation of the Knudsen theory requires that the equilibrium in the cell is not disturbed by the introduction of the orifice. In fact, it is, and the system is not in equilibrium but in a steady state with material continually being transferred from the sample, through the cell, and out the orifice. This transfer may result in measured pressures somewhat lower than the saturated value.

Theoretically, this steady state may be treated by considering the cell itself as an orifice, with its own Clausing factor. Motzfeldt⁷⁴ has calculated the pressure gradient in real cells due to orifice loss, and a more rigorous treatment by Carlson⁷⁵ confirmed his work.

Experimentally, large deviations from equilibrium result in the so-called "orifice effect," in which a large change in orifice area is accompanied by an inverse change in the measured pressure at a given temperature. Carlson et al.⁷⁶ have suggested an empirical expression to correct the observed pressure to the equilibrium value, using the orifice area and sample area as parameters.

c. Viscous Flow

Another requirement of Knudsen theory is that loss of effusate does not alter the molecular velocity distribution in the vicinity of the orifice. This is true if the mean free path is large compared to the orifice diameter; that is, if there is negligible chance that a molecule will experience a collision in the vicinity of the orifice. At higher pressures, collisions produce a cooperative effect, the ideal gas

assumption (molecules of zero diameter) breaks down, and so-called "viscous flow " results. Knudsen⁷⁰ arbitrarily set the upper limit of "molecular flow" at a mean-free-path/orifice-diameter ratio of 10, but in practice it has been difficult, if not impossible, to predict a priori the onset of viscous flow for a given vapor and crucible design⁶⁸.

d. Small Knudsen Cells

In many cases the large mean free path necessary for molecular flow is larger than the dimensions of the Knudsen cell. In this case most molecules leave a surface and go through the orifice without experiencing gaseous collisions, and the concept of an "equilibrium gas" is rather strained. Fortunately, the cosine rule holds for molecules scattered from a wall or emitted from the sample, so some degree of randomness is maintained, although weak specular components of scattering have been observed in some special cases^{77,78}. This problem is considered in more detail by Ward⁷⁹.

e. Vaporization Coefficient

The vaporization coefficient, α , is defined as the ratio of the rate of evaporation of a sample to the rate of collision on its surface from its equilibrium vapor. Values of α may vary from 0 to 1, and are usually assumed to be unity unless there is evidence to the contrary, although cases of very low vaporization coefficients^{80,81,82} have been reported. Low coefficients are characteristic of a potential energy barrier to vaporization, usually due to markedly different molecular geometry in the vapor and condensed phases. The low rate of evaporation leads to undersaturation and a more marked "orifice effect", but all but the most severe cases may be treated using a small orifice and a finely divided sample⁸³.

f. Surface Diffusion

In general a molecule striking the wall of a Knudsen cell does not immediately bounce off, but is absorbed, migrates some distance, and is then re-emitted according to the cosine rule. Molecules which strike near the orifice may migrate to the outside of the cell and be re-emitted, adding a spurious component to the effusate. This effect has been observed in some cases⁸⁴ and treated theoretically by Winterbottom and Hirth^{85,86}. Unfortunately, parameters necessary to make corrections using this theory are not available. The effect is least significant for species whose residence time absorbed on the walls is short.

5. Practical Limitations of the Knudsen Method

a. Characterization of Condensed Phases

In assigning to the equilibrium constant the value of the vapor pressure, the assumption is made that all condensed species are at unit activity, that is, pure. There are several cases in which this assumption is not valid. In an incongruent vaporization, there is always some degree of mutual solubility of the two condensed phases. The container may interact with the sample, either raising or lowering the apparent pressure. Small amounts of dissolved impurities, especially oxygen⁸⁷⁻⁸⁹, have been shown to have drastic effects on vapor pressures, and such contaminants may even be produced in situ by reaction with residual gases if the system pressure is not kept sufficiently low. Extreme care must be exercised to assure that such effects are either absent or properly accounted for.

b. Diffusion-Limited Vaporization

In an incongruently vaporizing system the second phase tends to form on the outside of the vaporizing species, which must then migrate through it to the surface to enter the vapor phase. If the migration is slower

than losses through the orifice, undersaturation will result. This phenomenon is usually experienced as a trend of vapor pressure with time or particle size.

c. Container Losses

In some cases it has been shown that a significant fraction of the vapor molecules striking the container wall are permanently absorbed. Ward, et al., in experimental^{90,91} and Monte Carlo^{92,93,79} studies have shown that this absorption leads to a pressure gradient in the cell and marked deviation from the distribution predicted by the cosine law at high angles. However, in most cases the effusate collected on targets coaxial with the orifice vaporizes directly from the sample and if the vaporization coefficient is unity such losses appear not to affect this form of Knudsen effusion.

d. Collection Losses

For meaningful measurements it is important to analyze all molecules which leave the orifice within the solid angle defined by the target, and only those molecules. Implementation involves several requirements:

- (1) The mean free path outside the cell must be considerably larger than d , the orifice-to-target distance, so that no significant number of molecules undergo collisions and are scattered away from the target. Residual vacuums of 10^{-5} torr or better are required.
- (2) All effusate striking the target must adhere. Experiments have been designed⁹⁴ to measure the sticking coefficient.
- (3) Any effusate not striking the target must be permanently removed from the system. It must not be re-emitted from the vacuum chamber walls. Re-emission is particularly a problem when the condensed effusate is a conductor, e.g., a metal, and induction heating is employed.

e. Other Limitations

There are several other problems encountered in converting Knudsen theory to practice. Temperature gradients within the cell and their effects⁹⁵ must be avoided. Just as important, the temperature must not drift with time as a sample is collected. Thermal expansion of the orifice must be considered, but Kent⁹⁶ has shown its effects to be negligible. Mass spectrometry has made characterization of the vapor phase much more straightforward than characterization of the condensed phase (section III,B,5,a) but the spurious effects of fragmentation still must be considered.

6. Temperature Measurement

The International Practical Temperature Scale of 1948 defines⁹⁷ temperatures above 1336 K by the intensity of radiation by a black-body according to the Planck Radiation Law. This intensity is measured by optical comparison with the filament of a standard lamp in an optical pyrometer⁹⁸. Corrections must be applied for absorption and reflection of light by the optical elements in the system. The correction is derived⁹⁹ from Wien's law and given by equation (III-11),

$$\frac{1}{T} - \frac{1}{T_a} = \frac{\lambda \ln \tau}{c_2} = \Delta\left(\frac{1}{T}\right) \quad \text{III-11}$$

where T_a is the apparent temperature, τ is the transmissivity of the optical elements, c_2 (1.438 cm K) is the second fundamental radiation constant and λ is the effective wavelength at T . Use of filters and the normal cutoff of the human eye makes λ , and thus $\Delta(1/T)$, nearly independent of T . Values of $\Delta(1/T)$ for various components are additive as a consequence of Beer's Law. Correction for a non-black body may be made by including the emissivity ϵ at wavelength λ , as in equation (III-12).

$$\frac{1}{T} - \frac{1}{T_a} = \frac{\lambda \ln \tau \epsilon}{c_2} \quad \text{III-12}$$

7. X-Ray Fluorescence Analysis

Atoms in excited electronic states may return to lower states by filling the vacancy from an outer orbital and emitting electromagnetic radiation of an energy characteristic of the element. Primary radiation results when the excited state is created by an electron beam. If it is created by a gamma ray or X-ray, secondary or fluorescent radiation results. Fluorescent radiation involving inner orbitals is in the X-ray region of the electromagnetic spectrum, and is simple and practically insensitive to chemical environment. Highly sensitive, non-destructive quantitative and qualitative analysis may be accomplished¹⁰⁰ by energy analysis of this radiation.

Wavelength-dispersive analysis uses the principle of X-ray diffraction as given by the Bragg equation, (III-13). With the interplanar distance d

$$n\lambda = 2d \sin \phi \quad \text{III-13}$$

fixed for a given analyzing crystal, photons of different wavelength, λ , and hence energy, are diffracted at different angles ϕ .

C. Thermodynamic Data Reduction

1. Second Law Calculations

The Gibbs free energy is defined⁶⁷ by equation (III-14), so at

$$G = H - TS \quad \text{III-14}$$

constant temperature equation (III-15) will hold. Combining (III-15)

$$\Delta G_T^\circ = \Delta H_T^\circ - T\Delta S_T^\circ \quad \text{III-15}$$

with equation (III-4) and rearranging gives equation (III-16). To the

$$\ln K_T = \frac{-\Delta H_T^\circ}{RT} + \frac{\Delta S_T^\circ}{R} \quad \text{III-16}$$

extent that ΔH_T° and ΔS_T° are independent of T , this is the equation of a straight line in $\ln K_T$ and $1/T$. Treatment of experimental $\ln K_T$ versus $1/T$ data by linear least squares gives the slope, a, and intercept, b,

from which $\Delta H_T^\circ = -Ra$ and $\Delta S_T^\circ = Rb$ may be obtained.

If the heat capacities of the reactants and products are known or can be estimated, the thermochemical values may be corrected to the reference temperature 298 K by equations (III-17) and (III-18). The

$$\Delta H_{298}^\circ = \Delta H_T^\circ + \int_T^{298} \Delta C_p dT \quad \text{III-17}$$

$$\Delta S_{298}^\circ = \Delta S_T^\circ + \int_T^{298} \frac{\Delta C_p dT}{T} \quad \text{III-18}$$

term ΔC_p is the heat capacity difference between the products and reactants.

Although the value of T to which the line (III-16) corresponds is not well established¹⁰¹, the experimental median temperature T_m is usually used. Also, since ΔC_p for the reaction over the temperature range of the measurements is generally non-zero, the data should exhibit slight curvature. Both these difficulties are overcome by the Σ -plot treatment, which incorporates heat capacity equations⁶⁷ or tabulated thermodynamic data¹⁰² and gives ΔH_{298}° directly.

2. Third Law Calculations

The free energy function (fef), as defined in equation (III-19), is

$$\text{fef}_T = (G_T^\circ - H_{298}^\circ)/T \quad \text{III-19}$$

a smooth function of temperature and may be extrapolated with a high degree of precision. The function can be calculated directly for gases when the spectroscopic energy levels are known⁶⁷. Rewritten as in equation (III-20), it may be calculated from tabulated or estimated

$$\text{fef}_T = \frac{H_T^\circ - H_{298}^\circ}{T} - (S_T^\circ - S_{298}^\circ) - S_{298}^\circ \quad \text{III-20}$$

entropies and heat capacities with the aid of equations (III-17) and (III-18).

For a reaction Δfef is the difference between the fef of the products and that of the reactants. The definition can be combined with equation

(III-4) and rearranged to give equation (III-21). Each experimental

$$\Delta H_{298}^{\circ} = -T(\Delta f_{ef} + R \ln K_T) \quad \text{III-21}$$

vapor pressure measurement may be treated by the third law method to give a value of ΔH_{298}° .

The individual third law values may be examined for consistency and trend, either with temperature or chronological sequence. A temperature trend indicates a systematic error in temperature or pressure measurement or in the thermodynamic functions employed. Agreement between second- and third-law enthalpies is also used as a check of the measurements, the definition of the vaporization process, and the thermodynamic values. Such agreement ensures only internal consistency, not absolute accuracy, and should be used with care since the two measures of enthalpy are slightly correlated¹⁰¹.

3. Derived Thermodynamic Quantities

The results of vaporization measurements may be used to obtain the energetics of formation of the reactant if the values for the products are known. For any reaction equation (III-22) holds, with i and j

$$\Delta H_{298}^{\circ} = \sum_i \nu_i \Delta H_{f298i}^{\circ} - \sum_j \nu_j \Delta H_{f298j}^{\circ} \quad \text{III-22}$$

referring to products and reactants, respectively, in equation (III-2).

Since for a vaporization there is only one reactant, it may be simplified as in equation (III-23). Identical expressions are valid for ΔG_{f298}°

$$\Delta H_{f298j}^{\circ} = \frac{1}{\nu_j} (\sum_i \nu_i \Delta H_{f298i}^{\circ} - \Delta H_{298}^{\circ}) \quad \text{III-23}$$

and ΔS_{f298}° .

Comparison with ΔH_{f298}° measured by other methods (e.g., combustion calorimetry) gives a check on the vaporization results.

The second law entropy change ΔS_{298}° may be compared with the value calculated from absolute entropies if such values are available. Conversely,

it may be used to calculate an absolute entropy for one of the constituents whose low temperature heat capacity has not been measured. Thorn and coworkers¹⁰³⁻¹⁰⁷ have used absolute entropies and a correlation between experimental enthalpy and entropy to choose a "best" value of enthalpy, but there exists controversy¹⁰⁸⁻¹¹⁰ whether the correlation is a physical phenomenon or an artifact introduced by the mathematical treatment.

If ΔG_{f298}° are known, they may be compared with the results of the vaporization, but no more information is gained than from comparisons of ΔH_{f298}° and ΔS_{f298}° directly.

CHAPTER IV

EXPERIMENTAL METHODS

A. Materials

Chemicals and materials used: (a) samarium and thulium metal, 99.9%, Michigan Chemical Corp., St. Louis, MI; (b) samarium sesquioxide and thulium sesquioxide, 99.9%, Michigan Chemical Corp., St. Louis, MI; (c) graphite powder, Grade No. 38, Fisher Scientific Co., Fair Lawn, NJ; (d) graphite rod, spectrographic grade, Becker Brothers Carbon Co., Cicero, IL; (e) tantalum seamless tubing, Fansteel Corp., North Chicago, IL; (f) molybdenum powder, 325 mesh, Fansteel Corp., North Chicago, IL; (g) molybdenum rod, Kulite Tungsten Corp., Ridgefield, NJ; (h) catalyst R3-11, Badische Anilin und Soda Fabrik, AG, Ludwigshafen am Rhein, Germany; (i) Ascarite, A. H. Thomas Co., Philadelphia, PA; (j) hydrochloric acid, reagent; and (k) potassium chloride, reagent, annealed at 350°.

B. Preparation

Samples for effusion experiments were prepared by direct combination of the elements in sealed tantalum ampoules. Seamless tantalum tubing was outgassed in vacuum at >2000° for at least two hours, then one end was crimped and sealed by arc welding in an atmosphere of argon or helium. The graphite was also outgassed at >2000° in vacuum before use. Samarium metal was handled in a glove box, but this was not necessary for thulium. The metals were chipped from the ingots and weighed into the ampoule with a 5-10%

excess of graphite over that required for the dicarbide stoichiometry. The other end of the ampoule was then crimped and welded in the same manner. The welding chamber was evacuated twice to <0.2 torr and flushed with the welding gas before each weld, and then a zirconium button was melted to remove any remaining traces of oxygen.

The sealed ampoules were heated inductively in vacuum to 1400-1600° for 2-6 hours, then cooled and transferred to the glove box.

C. Sample Handling

All tantalum ampoules were opened in the argon-filled glove box. For early experiments this box was dried using open dishes of phosphorus pentoxide. For SmC_2 vaporization experiments 16A, 16B, and 16C it was dried by recirculating the argon through activated alumina and deoxygenating catalyst R3-11. The two towers of alumina were alternately regenerated at 425°.

Knudsen crucibles were placed in a ground glass weighing bottle for transfer to the vaporization apparatus, which was flushed with argon during the time required for assembly. After vaporization experiments the evacuated system was filled with argon and the same techniques were used to return the crucibles to the glove box port.

Samples for Guinier X-ray powder diffraction or for mass spectrometry were coated with light paraffin oil to prevent hydrolysis during transfer.

D. Chemical Analysis

1. Free Carbon Analysis

Analysis of unreacted graphite was effected by direct weighing of the residue of hydrolysis. Samples were hydrolyzed and dissolved

in 20 ml 3M hydrochloric acid, digested, and filtered into constant weight sintered glass crucibles. The precipitate was dried at 110° and weighed.

2. Thulium and Samarium Analysis

Metal content was analyzed gravimetrically by direct conversion to the sesquioxide. Samples were weighed into constant weight crucibles in the dry box. Some were charred with a bunsen burner and then ignited at 950° in a muffle furnace. Others were slowly heated to 950° in a tube furnace under a flow of pure oxygen.

Attempts were made to analyze for metal content with the solutions left over from determination of free carbon. They were adjusted to pH 4 with sodium hydroxide and the metal oxalate was precipitated by adding saturated oxalic acid solution. The oxalate precipitate was filtered into constant weight alundum crucibles and fired to the sesquioxide. This method gave lower results and poor precision.

3. Total Carbon Analysis

When metal analysis was performed in the tube furnace, the gaseous products were passed over CuO and CeO_2 at 750° to catalyze conversion to CO_2 , dried by passing over MgClO_4 , and collected on Ascarite. The total carbon content was determined gravimetrically as carbon dioxide.

4. Oxygen Analysis

For the samples on which both metal and total carbon analysis were done, oxygen content was determined by difference.

E. X-Ray Diffraction

Samples were examined by X-ray powder diffraction before and after vaporization experiments. Debye-Scherrer ($\text{Cu K}\alpha$) and forward-focussing Guinier-Hägg ($\text{Cu K}\alpha_1$) cameras were employed. Methods for aligning the Guinier camera are outlined in Appendix I. Sample preparation and film measurements were essentially identical to those described by Haschke⁹⁴ and Stezowski¹¹¹. Annealed potassium chloride ($a_0 = 6.29300 \pm 0.00009 \text{ \AA}$)¹¹² was used as an internal standard. Diffraction data were reduced with the aid of the linear regression program of Lindquist and Wengelein¹¹³.

F. Mass Spectrometry

A Bendix Model 12 time-of-flight mass spectrometer modified to include a Knudsen source was used to identify the species in the vapor over TmC_2 . A tantalum crucible with a channel orifice, of the design described by Pilato²⁶, was heated by electron bombardment. Both continuous and pulsed ionization modes were used, with ionizing potentials of up to 55 ev. Appearance potential data were obtained by a linear extrapolation technique using mercury and nitrogen as internal standards.

Since it is well documented^{24-26,45} that Sm(g) is the only vapor species in the equilibrium with SmC_2 , no mass spectrometric investigation was made of the SmC_2 vaporization.

G. Target Collection Techniques

The target collection apparatus used in these measurements has been described previously by Kent⁹⁶ and Haschke⁹⁴. The targets were aluminum discs with a recessed collection surface, which was polished with 600 mesh emery paper, then cleaned with dilute HCl and distilled water before use. The target magazine was liquid nitrogen cooled. Haschke⁹⁴ has shown that monatomic metal vapors have unit sticking coefficient on such targets.

Crucible to target distances were measured with a cathetometer after the magazine was cooled. They varied from 10.4 to 12.3 cm. Effusion cells of the two designs described by Haschke⁹⁴ were fashioned from molybdenum. Areas of the nearly knife edge orifices were measured with a compensating polar planimeter (Keuffel and Esser Co.) from 100x photomicrographs made with a Bausch and Lomb Dynazoom metallograph.

A 20-kva Thermonic high-frequency induction generator was used to heat the effusion cells. Targets were exposed with both increasing and decreasing temperatures. By replacing the target magazine with an optical window it was determined that the temperature gradient between the upper and lower black-body cavities was less than 5 degrees.

H. X-Ray Fluorescence Analysis

1. Spectrometer Operation

Exposed targets from effusate collection experiments were analyzed by X-ray fluorescence by use of a Siemens goniometer with 4b spectrometer attachment, LiF analyzing crystal, NaI(Tl) scintillation detector, and a tungsten anode X-ray tube powered by a Siemens Kristalloflex 4 generator. Operation parameters were optimized for Sm $L\beta_1$ and Tm $L\alpha_1$ radiation according to the criteria set forth by Neff¹¹⁴. Impurities in the aluminum targets gave a peak which interfered with the Sm $L\alpha_1$ radiation. Counting and scanning procedures developed by Haschke¹¹⁵ were used.

2. Spectrometer Calibration

Standard targets were prepared from solutions of the sesquioxide. Calcined Tm_2O_3 or Sm_2O_3 was weighed on a semi-micro balance, dissolved in a minimum of 6M HCl, and diluted volumetrically to give solutions containing 50 to 150 μg metal/ml of solution. These solutions were placed on targets identical to those used for effusate collection, with

an ultra-precision micro buret (Kontes Glass Co.). The targets were dried over phosphorus pentoxide and counted in the usual manner. Least squares analysis of the counts was used to obtain the sensitivity per microgram of rare earth metal. The calibration was linear between 0.5 and 15 μg .

I. Temperature Measuring Equipment

Temperature measurements were made with a National Bureau of Standards-calibrated Leeds and Northrup disappearing filament optical pyrometer (serial number 1572579). Prism and window transmissivities were measured by observations of a tungsten strip lamp powered from a constant voltage source. Corrections were made using the average value of $\Delta(1/T)$ from observations at several temperatures. Temperature measurements for preparative reactions in tantalum bombs were corrected for the emissivity of tantalum (0.49 at 650 $\text{m}\mu$).

J. Specific Experimental Conditions

Pressure measurements were made at successively increasing and decreasing temperatures in the range 1630–2050 K for SmC_2 and 1660–2130 K for TmC_2 . Orifice areas ranged from 7.2×10^{-4} to $39.2 \times 10^{-4} \text{ cm}^2$ for the Sm-C measurements and from 11.8×10^{-4} to $64.0 \times 10^{-4} \text{ cm}^2$ for the Tm-C measurements. Under these conditions 3.0 – 15.0 μg of metal was collected on each target in times ranging from 2.0 to 60 minutes. The cells were charged with 0.25 – 0.65 g samples. Residual pressure in the system was maintained at 10^{-5} to 10^{-6} torr with a mercury diffusion pump and mechanical forepump.

High-carbon compositions were studied by mixing weighed amounts of outgassed graphite with the dicarbide before loading it into the cell (runs 11, 15, 16A, 16B and 16C for Sm; 13 and 14 for Tm). Tests for container

interaction were made by placing the sample in a graphite cup inside the molybdenum cell (run 12 for Sm) or by using an equimolar mixture of SmC_2 , graphite, and 325 mesh molybdenum powder to charge the cell.

A test to confirm contaminant interaction was made as follows. In experiment 16 a sample of SmC_2 was mixed with graphite and vaporized (16A) in the normal manner. It was then stored with the special handling techniques described in section IV, C, for the minimum time required to prepare the apparatus for a new experiment (16B). After experiment 16B, it was stored again with the same precautions, for a similar minimum time, but this time, 17 mg calcined Sm_2O_3 was added. This intentionally contaminated sample was used for experiment 16C.

CHAPTER V

RESULTS

A. Preparative

All preparations of SmC_2 yielded a golden-colored powder, which was sometimes slightly sintered. This product was extremely hygroscopic, and produced the sharp odor associated with acetylene when it decomposed to a grey powder in the presence of traces of moisture. In spite of the precautions described in section IV,C, attempts to store this material for more than a few weeks were generally unsuccessful.

Preparations of TmC_2 yielded a similar golden-colored product when cooled quickly, or a black powder when cooled over a period of more than two hours. Both these preparations were quite hygroscopic, but not to the degree of SmC_2 .

B. Analytical

1. Chemical Analysis

Samples of both SmC_2 and TmC_2 were found to be generally metal-rich, $1.78 \leq \text{C/M} \leq 2.02$, even though all samples also had unreacted graphite present, in amounts which varied from 1.2 to 1.7 weight per cent. Combined metal and total carbon analysis typically recovered around 99.2% of the sample, so contamination, considered to be oxygen, was about 0.8% by weight.

2. X-Ray Powder Diffraction Analysis

The X-ray powder diffraction patterns of the golden-colored forms of SmC_2 and TmC_2 showed them to be body centered tetragonal, isostructural with CaC_2 , as reported by Spedding et al.⁴ The black form of TmC_2 gave an X-ray powder diffraction pattern which matched that of the low temperature modification of the dicarbides reported by Krupka et al.¹⁹

The very complex diffraction pattern of the black form of TmC_2 has not yet been indexed satisfactorily on the basis of a single phase. An attempt was made to prepare single crystals by annealing and to determine the crystal structure. The resulting crystals were not sufficiently well formed for structure determination purposes, but examination of their Weissenberg X-ray photographs indicated that two phases were present. One phase, indexed on orthorhombic symmetry, has a much smaller volume than the cell proposed by Krupka et al. and accounted for most of the powder diffraction lines. The other phase, indexed on hexagonal symmetry on the basis of single crystal diffraction data, showed the rather stringent reflection requirements hkl , $h + k \pm l = 3n$; $00l$, $l = 6n$. This phase accounted for seven more of the powder diffraction lines, the only lines allowable under the aforementioned restrictions. Six of the remaining ten lines matched the strongest lines from the known impurities, graphite, tetragonal TmC_2 , and TaC . The remaining four lines, all weak, were accounted for by relaxing the $k + l = 2n$ restriction indicated by the single crystal X-ray photographs of the orthorhombic phase. The lattice parameters of these phases, along with the observed lattice parameters of the tetragonal SmC_2 and TmC_2 structures, are listed in Table 2. The observed intensities,

interplanar d-spacings, and their assignments are listed in Appendix II.

The black mixture of phases converted immediately to the tetragonal dicarbide upon heating in vacuum.

Table 2

Observed Lattice Parameters of Phases Prepared in This Study

Compound	<u>a</u>	<u>b</u>	<u>c</u>
Tetragonal SmC ₂	3.79 ± 0.02* Å		6.37 ± 0.04 Å
Tetragonal TmC ₂	3.6026 ± 0.0004		6.056 ± 0.001
Orthorhombic "TmC ₂ "	3.68 ± 0.01	12.40 ± 0.04 Å	13.58 ± 0.03
Hexagonal "TmC ₂ "	3.19 ± 0.01		16.74 ± 0.07

*The indicated uncertainties are calculated standard errors.

C. Mass Spectrometry Results

1. Vaporization Mode

In the mass spectrometric investigation of the TmC₂ vaporization, Tm⁺ (at m/e = 169) was the only shutterable peak in the region 160 ≤ m/e ≤ 210 when a 30 or 55 ev ionizing electron beam was used. Limits were set for carbide vapor species at I_{TmC₂}⁺ < 0.005 I_{Tm}⁺ and I_{TmC}⁺ < 0.02 I_{Tm}⁺. The presence of a background peak at m/e = 181 decreased the sensitivity for TmC⁺.

These observations indicate that TmC₂ vaporizes according to reaction (V-1). It has already been indicated in section IV,F that SmC₂ vaporizes



by the analogous reaction (V-2). Second law treatment of seven (T, I_{Tm}⁺)



data points in the range 1855–2150 K gave $\Delta H_{\text{V}2000}^\circ = 64.0 \pm 2.7$ kcal/gfw.

2. Appearance Potential

From the ionization efficiency curves for Tm⁺, Hg⁺, and N₂⁺ shown in

Figure 1, appearance potentials of 10.1 volts for Hg^+ , 15.2 volts for N_2^+ , and 5.4 volts for Tm^+ were obtained. The literature values^{11,6} of 10.44 eV for Hg^+ from Hg and 15.56 eV for N_2^+ from N_2 allow correction to a value of 5.7 eV for Tm^+ with an estimated error of ± 0.2 eV. This value is in good agreement with the literature reports which vary from 5.81 to 6.51 eV for Tm(g) as the parent species, further confirmation that reaction (V-1) represents the vaporization mode of $\text{TmC}_2(\text{s})$.

D. Vaporization Results

1. Behavior of Metal-Rich Samples

No unusual vaporization behavior was noted for samples with $\text{C/M} < 3$. Metal rich samples first showed high erratic pressures which stabilized part way through a run. From the rate of metal loss and the chemical analysis of the sample it was possible to calculate the composition at any time. These calculations indicated that stable pressures were achieved very close to the $\text{MC}_{2.00}$ composition. For samarium, the measured pressures were within the range reported by earlier workers.

2. Behavior of Carbon-Rich Samples

When excess graphite was added to the effusion samples ($3 < \text{C/M} < 12$) the behavior was different from that reported by earlier workers. Pressures were first high, then decreased after 2-3 hours of heating. Data collected during the first part of these experiments exhibited the lower enthalpy reported by earlier workers^{21,24,25}. The second part of the experiment, however, gave pressures identical to those measured from samples which contained little excess carbon. A typical example is experiment 11 (Figure 2) in which the data points are numbered in the order in which they were taken. Additional experiments showed that the behavior was dependent on elapsed time, not ascending or descending temperature.

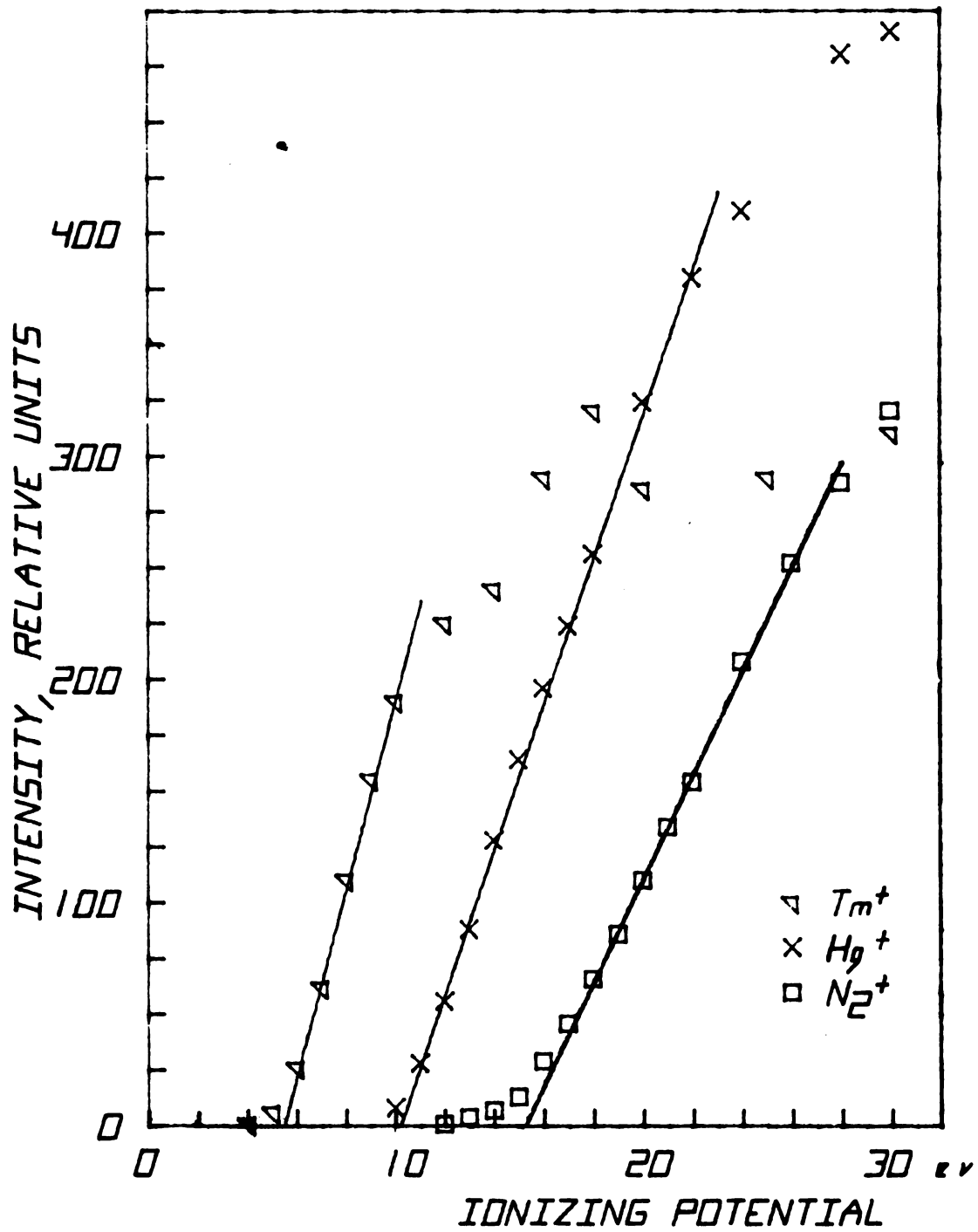


Figure 1. Ionization Efficiency Curves

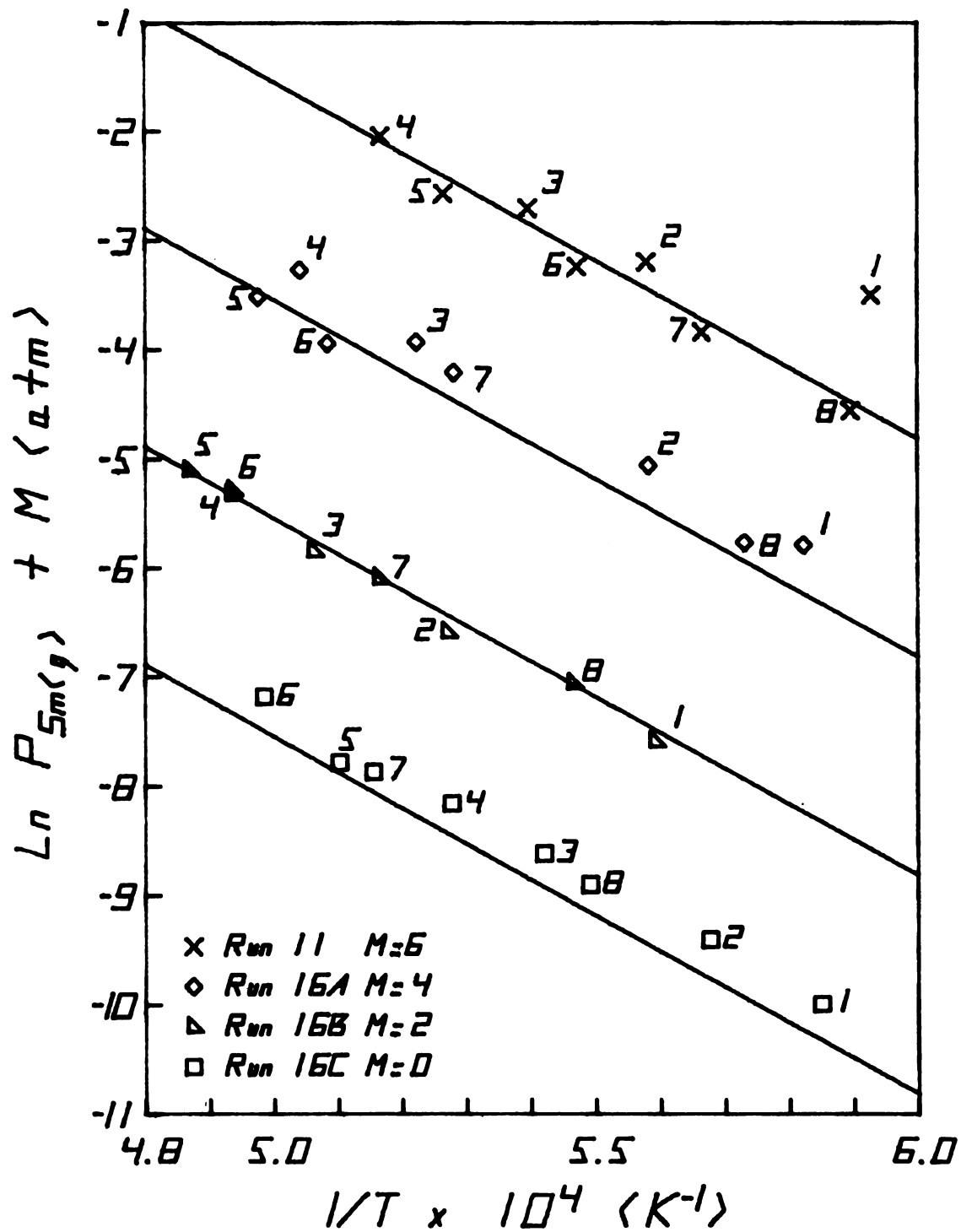


Figure 2. Vaporization Behavior of Carbon-Rich Samples

3. Container Interaction

The X-ray diffraction patterns of the samples after effusion were examined carefully. In two instances the three strongest lines of the Mo_2C pattern were observed, but even when 50% of the sample had been depleted these were among the weakest lines in the pattern.

Effusion of SmC_2 from a molybdenum cell fitted with a graphite liner (Run 12) gave results almost identical to those of experiment 11 (Figure 2) in which a high carbon content sample was effused from an unlined cell. The two experiments in which molybdenum powder was added to the sample did not show the initial high pressures. These samples had little excess carbon ($3 < \text{C/Sm} < 4$) and gave the same pressures, within experimental error, as the near-stoichiometric samples discussed in section V,D,1. It was concluded that container interaction, although present, does not significantly affect the vapor pressure of the metal in equilibrium with the dicarbide.

No change in pressure was observed when the orifice area was varied by a factor of six. This observation indicates that the cell lid was impervious to the diffusion of metal and that significant undersaturation (cf. III,B,4,b) was not present. Vapor pressures were kept below 0.6 torr to avoid the effects of viscous flow (cf. III,B,4,c).

4. Evidence of Contaminant Interaction

Two significant features were observed during the first part of high-carbon effusion runs, that is, the part where the measured pressures were higher than expected. First, the residual pressure in the vacuum system was also somewhat higher than usual. Second, for TmC_2 -C samples,

the duration of the first part of the run was related to the duration of storage of the sample, and this initial high pressure region could nearly be eliminated by using freshly prepared TmC_2 and freshly outgassed graphite. It has already been noted (Section V,A) that TmC_2 was observed not to be as susceptible to hydrolysis as SmC_2 .

In one experiment with a high carbon content sample the crucible was heated rapidly, and a very high system pressure resulted. A Tesla coil was used to excite a discharge in the residual gas. The color of the discharge - light blue - was attributed to carbon monoxide. Presence of this gas indicated contamination by an oxygen-containing species, which was reduced by the graphite.

When the mass spectrometric experiment was done, such a contamination effect was just beginning to be suspected, and the $m/e = 28$ peak was monitored during initial heating. When the system pressure rose, the $m/e = 28$ peak increased and the H_2O^+ peak at $m/e = 18$ did not. However, it was not confirmed (e.g., by fragmentation to C^+) that this increase was due to CO and not to N_2 . Appearance potential data for N_2 were taken well after the pressure returned to its base value.

5. Confirmation of Contaminant Interaction

The results of series 16 (cf. IV,J) are shown below those of experiment 11 in Figure 2. The line with each set of points indicates the pressure finally assigned for the equilibrium vaporization of $\text{SmC}_2(\text{s})$. Experiment 16A was qualitatively similar to experiment 11, although the scatter was somewhat greater than usual. Points 5, 6, 7, and 8 are within 2.5σ , or 99% confidence level, of the line, while points 1, 2, 3, and 4 are all above the line by $3.5\text{--}4.5\sigma$. A high residual system pressure (circa 1×10^{-4} torr) was observed during the exposure of targets 1-4.

The sample used in experiment 16B was still in the same composition range, but extreme care was taken to insure that no more oxygen reacted with it. There was a brief pressure surge in the system as the cell was heated to about 1350°, but it lasted less than the time normally allowed for equilibration. The measured vapor pressures were in excellent agreement with those represented by the line.

In experiment 16C the only difference from 16B was the intentional contamination with 17 mg Sm_2O_3 . The residual system pressure was high throughout experiment 16C, and all pressure data from it deviate positively from the equation finally assigned, five of them by $>2.5\sigma$. Thus the effect noted in the first part of the high-carbon content experiments is identical to that which results from addition of small amounts of oxide.

6. Vapor Pressure Equations for SmC_2

All SmC_2 target collection data points shown in Figure 3 were collected when oxygen contamination was absent. The linear least squares equation which describes the 62 data points ($1630 \leq T \leq 2050\text{K}$) is given by equation (V-3), where the uncertainties are calculated standard errors.

$$\ln P_{\text{Sm}}(\text{atm}) = [(-32,740 \pm 460)/T] + (8.84 \pm 0.25) \quad \text{V-3}$$

The pressures represented by equation (V-3) for the vaporization of $\text{SmC}_2(\text{s})$ are in very good agreement with the values reported by Faircloth et al.²¹, whose work was done by target collection on almost stoichiometric samples, and that portion of the work of Cuthbert, et al.²⁴ done by target collection. Oxygen contamination was undoubtedly present both in their work and in the portions of this study done on nearly stoichiometric samples, but its effect of high initial pressures and low enthalpies is similar to the effect of sesquicarbide usually present in dicarbide preparations, an effect which was recognized and allowed for.

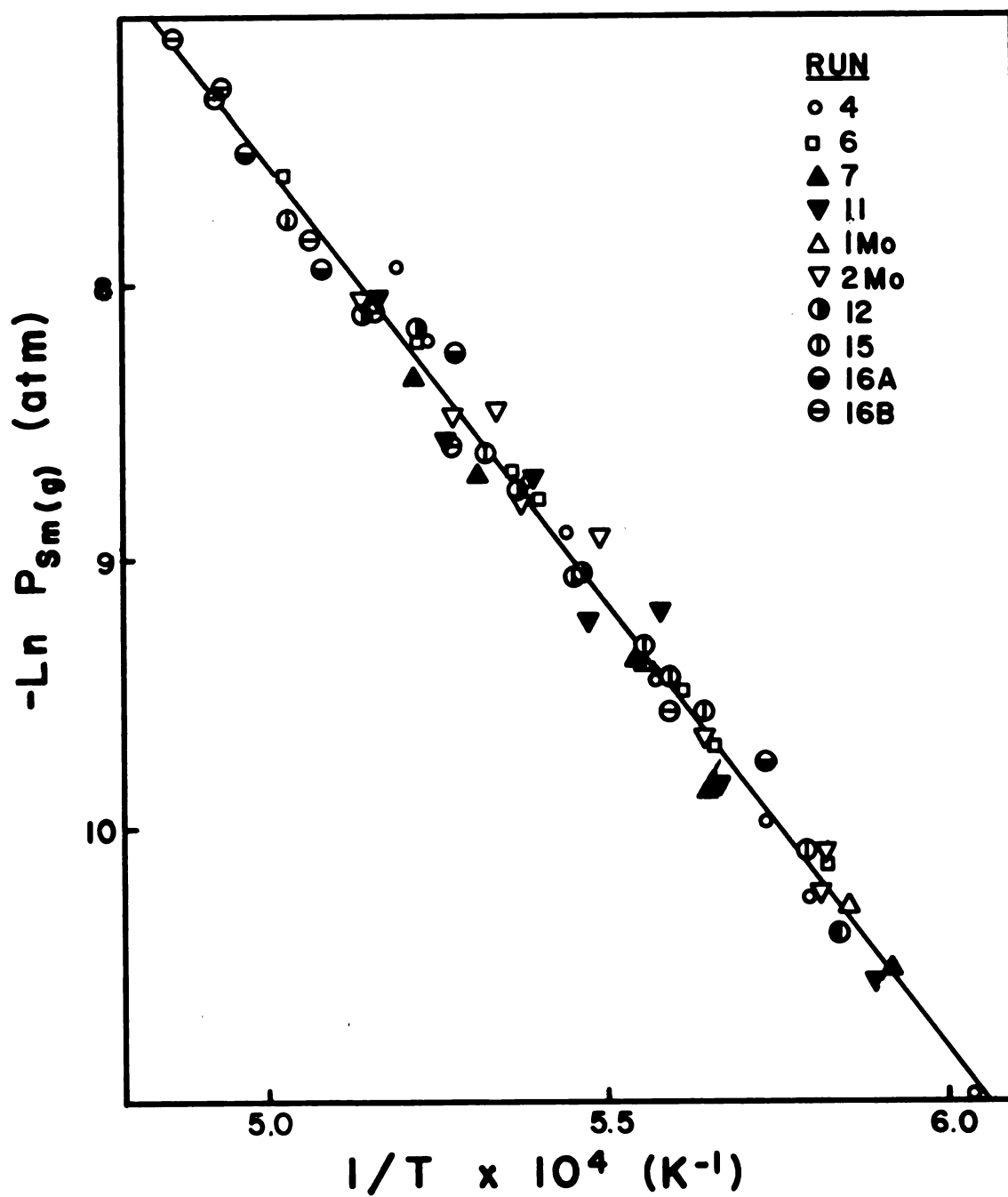


Figure 3. Equilibrium Pressure of Samarium Vapor Over Samarium Dicarbide

Since these three independent measurements of the Sm pressure in equilibrium with $\text{SmC}_2(\text{s})$ are in such good agreement, the best expression would be derived by combining all three studies. Such an equation (V-4), was derived by combining into one set the data

$$\ln P_{\text{Sm}}(\text{atm}) = [(-31,520 \pm 300)/T] + (8.15 \pm 0.20) \quad \text{V-4}$$

collected in this study, the 56 data points reported by Faircloth et al., and a data set constructed with a random number generator to duplicate the equation, standard error, temperature range, and number of data points reported by Cuthbert, et al. This expression is believed accurate to within ± 0.20 in $\ln P$ throughout the temperature range of 1400–2080 K.

From equation (V-4) and the relationships in section III,C,1 the following thermodynamic values are calculated for reaction (V-2):

$$\Delta H_{\text{V}1740}^{\circ} = 62.63 \pm 0.60 \text{ kcal/gfw and } \Delta S_{\text{V}1740}^{\circ} = 16.19 \pm 0.40 \text{ eu.}$$

7. Vapor Pressure Equation for TmC_2

For TmC_2 (Figure 4) the linear least squares line which describes the 46 data points ($1660 \leq T \leq 2130$ K) collected when oxygen contamination was absent is given by equation (V-5), where the uncertainties

$$\ln P_{\text{Tm}}(\text{atm}) = [(-35,570 \pm 340)/T] + (8.98 \pm 0.18) \quad \text{V-5}$$

are calculated standard errors.

From equation (V-5) and the relationships in section III,C,1 the following thermodynamic values are calculated for reaction (V-1):

$$\Delta H_{\text{V}1895}^{\circ} = 70.68 \pm 0.68 \text{ kcal/gfw and } \Delta S_{\text{V}1895}^{\circ} = 17.85 \pm 0.36 \text{ eu.}$$

E. Thermodynamic Data Reduction

1. Thermodynamic Values Employed

a. Heat Capacity Functions

Measured values of the heat capacity of graphite⁵⁴ and values of the heat capacities of the gaseous metals calculated from spectroscopic

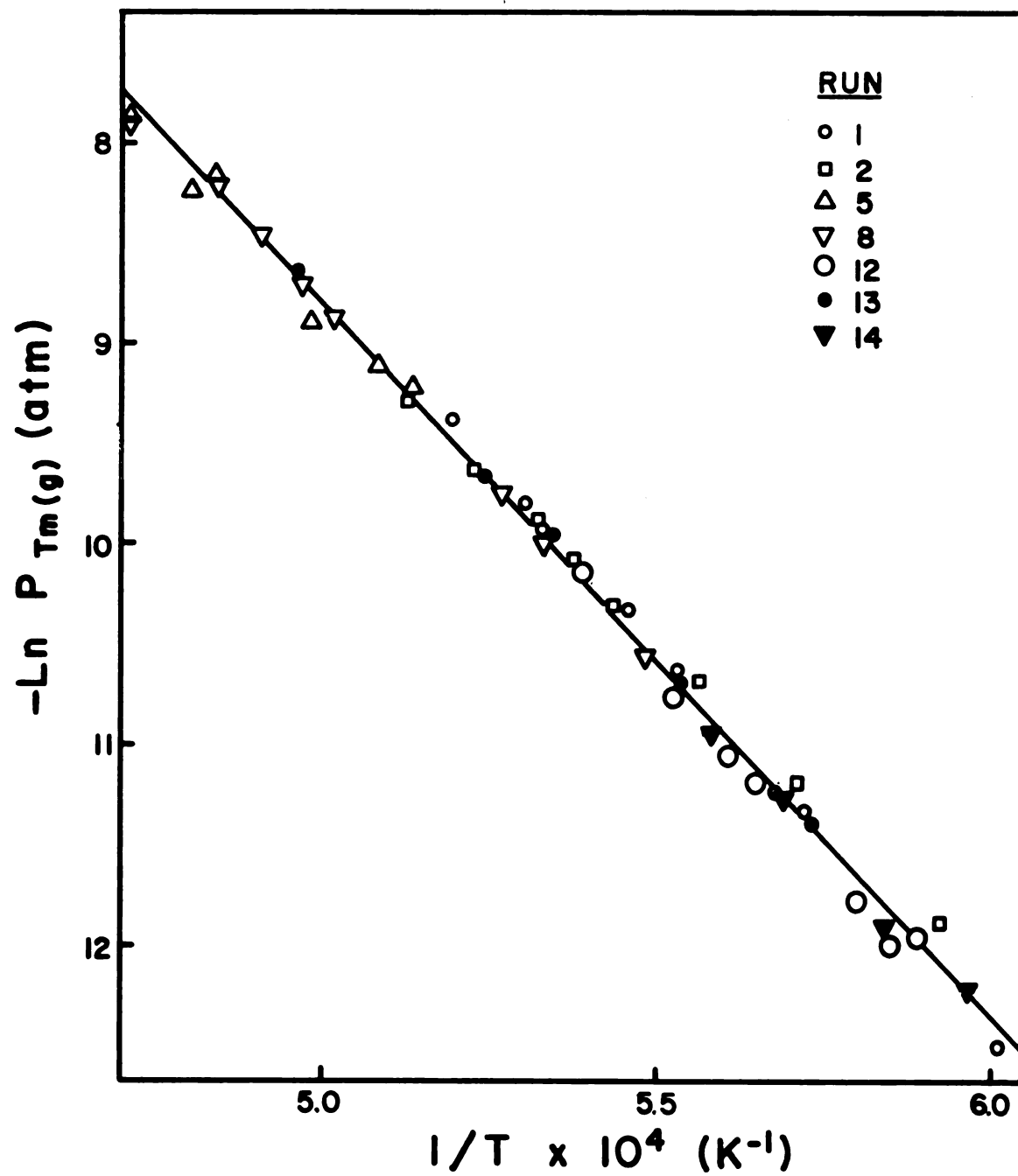


Figure 4. Equilibrium Pressure of Thulium Vapor Over Thulium Dicarbide

data^{117,118} were available. The heat capacities of SmC_2 and TmC_2 were assumed to be that of CaC_2 of the same crystal modification (cf. II,E). The $\Delta S_{\text{trans}}^\circ$ for the tetragonal to cubic conversion was assumed to be the same for all three carbides. From the enthalpy of transition for CaC_2 (1.33 kcal/gfw)⁵⁴ at 720 K, calculated values were $\Delta H_{\text{trans}}^\circ = 2.16$ kcal/gfw for SmC_2 and $\Delta H_{\text{trans}}^\circ = 2.50$ kcal/gfw for TmC_2 at their transition temperatures¹⁰ of 1170 and 1355 K, respectively.

From these heat capacity relationships, enthalpy and entropy increments were calculated using equations (III-16) and (III-17).

b. Absolute Entropies

Literature values were employed for S_{298}° of graphite⁵⁴, samarium vapor¹¹⁷ and thulium vapor¹¹⁸. An estimate of $S_{298}^\circ(\text{MC}_2)$ was made from $S_{298}^\circ(\text{CaC}_2) = 16.8$ eu⁵⁴ by subtracting Latimer's estimate¹¹⁹ of the calcium lattice contribution and adding the lanthanide lattice contribution¹²⁰ and a magnetic contribution $N \ln (2J+1)$. This calculation gave $S_{298}^\circ(\text{SmC}_2) = 25.2$ eu and $S_{298}^\circ(\text{TmC}_2) = 25.8$ eu. The estimating procedure is considered accurate to ± 1.5 eu.

c. Free Energy Functions

From the enthalpy and entropy increments and values of absolute entropy, free energy functions were calculated according to equation (III-20). The difference in free energy of the reactants and products, Δf_{ef} , was calculated for reactions (V-1) and (V-2) over the temperature range of the measurements and the results are tabulated in Appendix III.

d. Additional Thermochemical Values

In order to calculate enthalpies of formation of the dicarbides, the enthalpies of formation of the metal vapors were taken from Hultgren's compilation¹²¹. For calculations (section V,F) of the effect of oxide contamination on the apparent vapor pressure, the thermodynamic values

for the sesquioxides as reported by Holley, Huber and Baker¹²² were employed.

2. Results of Second Law Treatment

The thermodynamic values derived (cf. V,D,6 and V,D,7) from the pressure equations for reactions (V-1) and (V-2) were reduced to 298 K by use of the approximated heat capacity data. For the vaporization of $\text{SmC}_2(\text{s})$, $\Delta H_V^\circ 298 = 66.9 \pm 1.0$ kcal/gfw and $\Delta S_V^\circ 298 = 21.4 \pm 1.0$ eu. For the vaporization of $\text{TmC}_2(\text{s})$, $\Delta H_V^\circ 298 = 79.1 \pm 1.3$ kcal/gfw and $\Delta S_V^\circ 298 = 27.5 \pm 1.3$ eu. The error values indicate a composite of standard deviation and estimated error in the thermodynamic functions.

The values of $\Delta H_V^\circ 298$ have been combined with the enthalpies of formation of the gaseous metals¹²¹ at 298 K according to equation (III-23) to give $\Delta H_f^\circ 298 (\text{SmC}_2(\text{s})) = -17.5 \pm 1.3$ kcal/gfw and $\Delta H_f^\circ 298 (\text{TmC}_2(\text{s})) = -23.6 \pm 2.0$ kcal/gfw.

The experimental entropy of vaporization of SmC_2 compares well with the value calculated from the absolute entropies, 21.3 eu. The entropy value calculated for vaporization of TmC_2 , 22.3 eu, is not in satisfactory agreement with the experimental value.

3. Results of Third Law Treatment

The independent third law enthalpies, along with the pressure and temperature data from which they were calculated by equation (III-21), are shown in Appendix IV. The average value for SmC_2 was $\Delta H_V^\circ 298 = 66.5 \pm 3.0$ kcal/gfw, with no significant temperature dependence in the values.

The values for TmC_2 show a temperature trend of 2.3 kcal/gfw over the temperature range of the measurements, and their average, $\Delta H_V^\circ 298 = 69.1 \pm 4.0$ kcal/gfw, is not in satisfactory agreement with the second law value.

4. The Absolute Entropy of Thulium Dicarbide

It has been shown in the preceding two sections that the results for the vaporization of TmC_2 do not form a consistent set. Since it was believed that the disagreement was larger than could be explained by possible systematic errors in vapor pressure measurement, considerable attention was given to the thermochemical values and to other schemes for estimating them. From this study it was found that the discrepancy can be isolated in the $S_{298}^\circ(\text{TmC}_2)$ term. In particular, if this entropy is estimated by Latimer's method (cf. V,E,1,b), but no contribution for magnetic entropy is added, the following results are obtained:

- (1) The calculated entropy of vaporization is $\Delta S_V^\circ 298(\text{TmC}_2) = 27.4$ eu, in good agreement with the experimental second law value of 27.5 eu;
- (2) The average third law enthalpy is $\Delta H_V^\circ 298(\text{TmC}_2) = 78.7 \pm 3.0$ kcal/gfw, in good agreement with the second law value of 79.1 ± 1.3 kcal/gfw;
- and (3) there is no discernable temperature dependence in the third law data. Appendices III and IVB include the values calculated for TmC_2 both with and without a magnetic contribution to the estimated entropy.

Such internal consistency alone is not substantiating evidence for lack of a magnetic entropy contribution in TmC_2 , but independent confirmation is available. As has been indicated earlier (cf. II,B) Atoji¹⁷ has found by neutron diffraction that TmC_2 is the only lanthanide dicarbide studied which does not undergo an antiferromagnetic transition at low temperature. It is the entropy of this transition which is not observed in the vaporization results. Taken together, these observations strongly suggest that in the dicarbide environment the Tm^{+3} ion has a non-degenerate ground state, and that $S_{298}^\circ(\text{TmC}_2) = 20.7 \pm 1.2$ eu.

The results of thermodynamic data reduction are summarized in Table 3.

Table 3

Summary of Thermodynamic Results

SmC ₂	TmC ₂ , without magnetic entropy contribution	TmC ₂ , with magnetic entropy contribution
------------------	---	--

Second Law Values

Midrange Temperature	1740 K	1895 K
----------------------	--------	--------

ΔH_V° T	62.6 ₃ ± 0.6 ₀ kcal/gfw	70.6 ₈ ± 0.6 ₈ kcal/gfw
ΔH_V° 298	66.9 ± 1.0 kcal/gfw	79.1 ± 1.3 kcal/gfw
ΔS_V° T	16.1 ₉ ± 0.4 ₀ eu	17.8 ₅ ± 0.3 ₆ eu
ΔS_V° 298(exp)	21.4 ± 1.0 eu	27.5 ± 1.3 eu

Third Law Values

ΔH_V° 298	66.5 ± 3.0 kcal/gfw	78.7 ± 3.0 kcal/gfw	69.1 ± 4.0 kcal/gfw
------------------------	---------------------	---------------------	---------------------

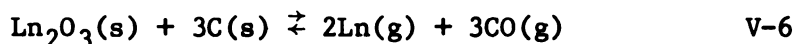
Derived Values

ΔH_f° 298(MC ₂)	-17.5 ± 1.3 kcal/gfw	-23.6 ± 2.0 kcal/gfw	
S_{298}° (MC ₂)	25.2 ± 1.5 eu	20.7 ± 1.2 eu	25.8 ± 1.5 eu
ΔS_V° 298(calc)	21.3 ± 1.5 eu	27.4 ± 1.2 eu	22.3 ± 1.5 eu

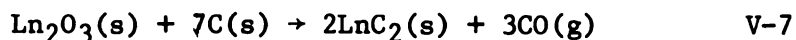
F. Thermodynamic Treatment of the Contaminant Reaction

1. The Reactions Involved

It has been proposed that the anomalous vaporization behavior of high carbon content samples was caused by the reduction of oxide-bearing contaminants by the graphite and the resultant increased metal pressures. It would be valuable to ascertain if such a reduction is thermodynamically feasible. Although the oxygen bearer may well have been one of the oxide carbides ¹²³⁻¹²⁵, it is informative to consider the thermodynamics of reduction of the lanthanide sesquioxide, reaction (V-6). The dicarbides



can be prepared by reaction (V-7) (cf. II,A), and microscopic examination



of quenched reaction mixtures revealed free metal. Since the sesquioxide can be expected to have higher oxygen activity than an oxide carbide, its reduction thermodynamics, as discussed in the next three sections, will indicate the highest possible metal pressure in such a system.

2. A Kinetically Controlled Vaporization

If under Knudsen conditions equation (V-6) has a higher equilibrium $\text{Ln}(\text{g})$ pressure than reaction (V-1) or (V-2), then reaction (V-8), the



reverse of the vaporization, can be expected to take place, and will lower the pressure of the lanthanide vapor. The observed pressure will not be an equilibrium value at all, but will depend on the relative rates of reactions (V-6) and (V-8). The pressure corresponding to (V-6) will be an upper bound on the observed value, and that corresponding to (V-1) or (V-2) will be a lower bound.

3. The Phase Rule

Reaction (V-6) is an example of vaporization of a ternary system, that is, $C = 3$. Since there are three phases, two solid and one gas, application of the phase rule leads to $F = 2$, and a vapor pressure equation will be meaningless unless another condition can be imposed. Fortunately, the mass balance requirement leads to a condition concerning the composition of the vapor. According to equation (V-6), two moles of metal vapor are produced for every three moles of carbon monoxide. Then at steady state, for every three moles of CO effused through the orifice, two moles of metal must either be effused or be consumed according to reaction (V-8). The principal loss is by effusion through the orifice, so equation (V-9), coupled with the Knudsen equation (III-7), gives for

$$\frac{W_{Ln}}{2M_{Ln}} = \frac{W_{CO}}{3M_{CO}} \quad V-9$$

the composition of the gas phase equation (V-10). Again, due to the

$$P_{CO(g)} = \frac{3}{2} \left(\frac{M_{CO}}{M_{Ln}} \right)^{1/2} P_{Ln(g)} \quad V-10$$

fact that $Ln(g)$ is also consumed by reaction (V-8), this equation represents an upper limit to $P_{Ln(g)}$, in agreement with the kinetic arguments presented in section V,F,2.

4. Results

The thermodynamics of reaction (V-6) can be considered in terms of equation (III-22) as a sum of the thermodynamics of formation of $Ln_2O_3(s)$, $CO(g)$, and $Ln(g)$, all of which are well characterized species^{121,122,126}. The ΔH_{298}° and Δf_{ef} for reaction (V-6) have been calculated for $Ln = Sm$, Tm and the third law procedure was used with equation (V-10) to calculate the Ln pressure.

The results for Sm are shown in Figure 5, along with the various reported values of P_{Sm} over SmC_2 . The equilibrium pressure over the oxide

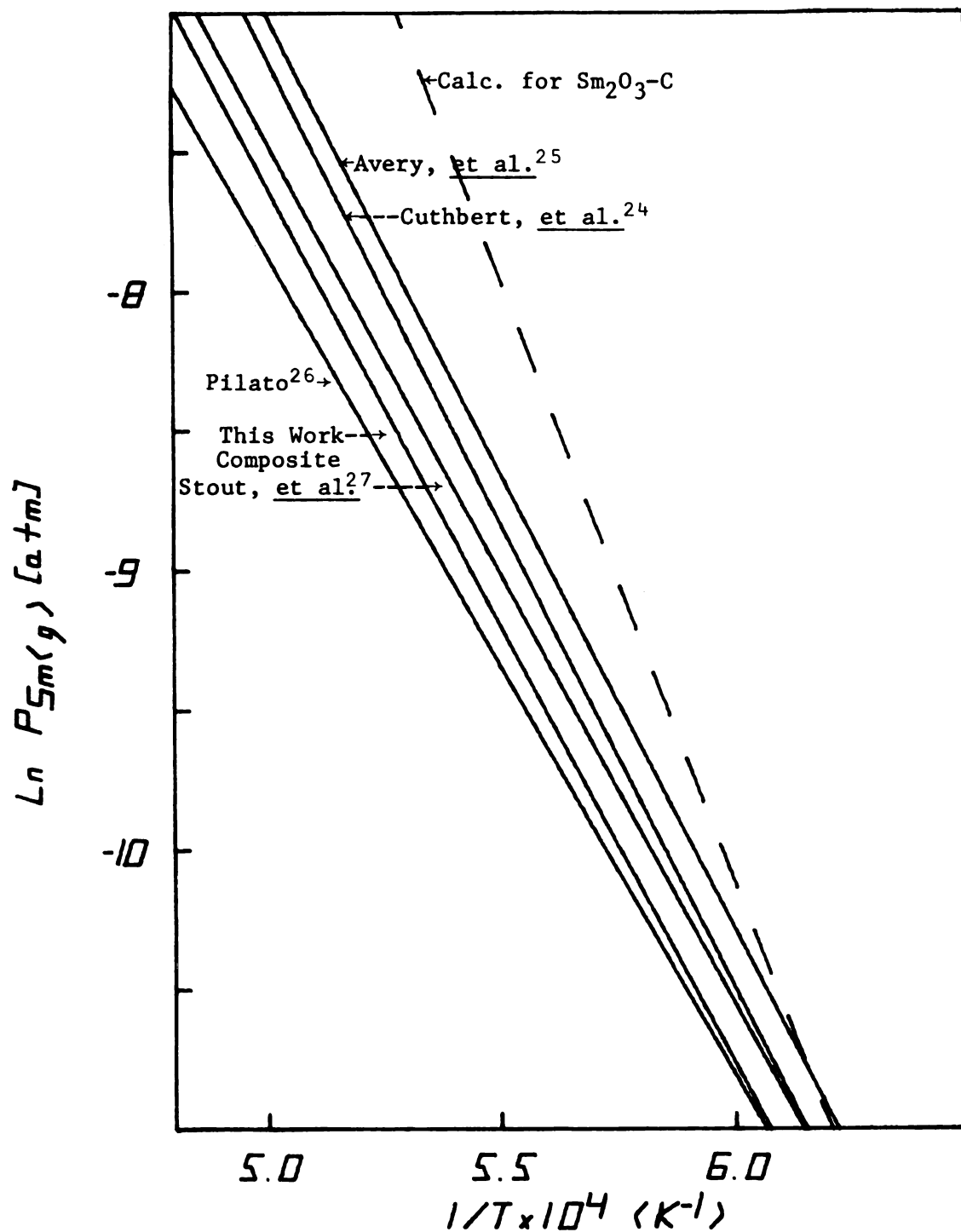


Figure 5. Equilibrium Samarium Pressure Reported for SmC_2 and Calculated for $\text{Sm}_2\text{O}_3\text{-C}$

mixture is higher than that over the dicarbide. Pressures observed over contaminated samples would be intermediate between the two values (cf. section V,F,2).

Likewise the results for Tm (Figure 6) show the same relationship. Thus it is thermodynamically feasible that oxide contamination of SmC_2 and TmC_2 caused the observed anomalies in the vaporization.

5. Extension to Other Lanthanide Dicarbides

The calculations described in the last section have been carried out for the other lanthanide elements to predict which other systems might be similarly affected by oxide contamination and to establish a criterion for evaluating conflicting reports of the decomposition pressures of other dicarbides. The results fall into three classes.

The calculation of ΔH_{298}° for reaction (V-6) is predominated by the enthalpy of formation of the lanthanide sesquioxide, which is relatively independent of the identity of the lanthanide. Thus P_{Ln} for reaction (V-6) is of the same order of magnitude for all the lanthanides. For the first class, the very refractory carbides, all CO(g) would be removed well before the temperature necessary for dicarbide vaporization was attained. No difficulties should be encountered in the vaporization of these dicarbides, with the possible exception of HoC_2 , which might be volatile enough to behave like SmC_2 and TmC_2 in the presence of oxide. Haschke³⁷ has noted that the enthalpy of vaporization of HoC_2 is not in line with those of the other dicarbides.

The second class includes the single carbide, YbC_2 , which is so volatile that its metal pressure is clearly greater than the pressure over a graphite-oxide mixture. This is shown in Figure 7. It should be noted that the higher Yb pressure will not drive reaction (V-6) to the left because there is no significant source of CO(g) . Thus Yb_2O_3 in a $\text{YbC}_2\text{-C}$

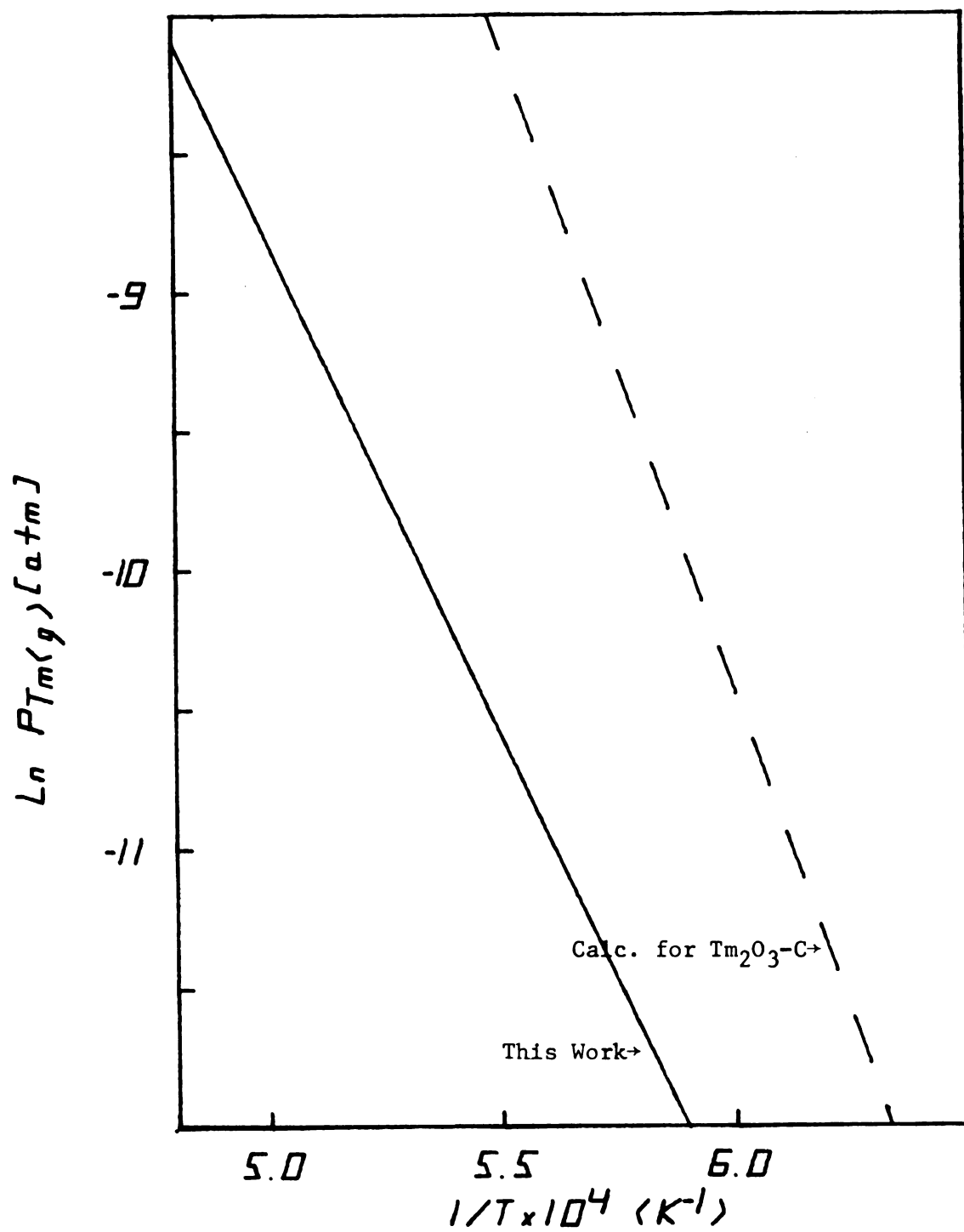


Figure 6. Equilibrium Thulium Pressure Reported for TmC_2 and Calculated for Tm_2O_3-C

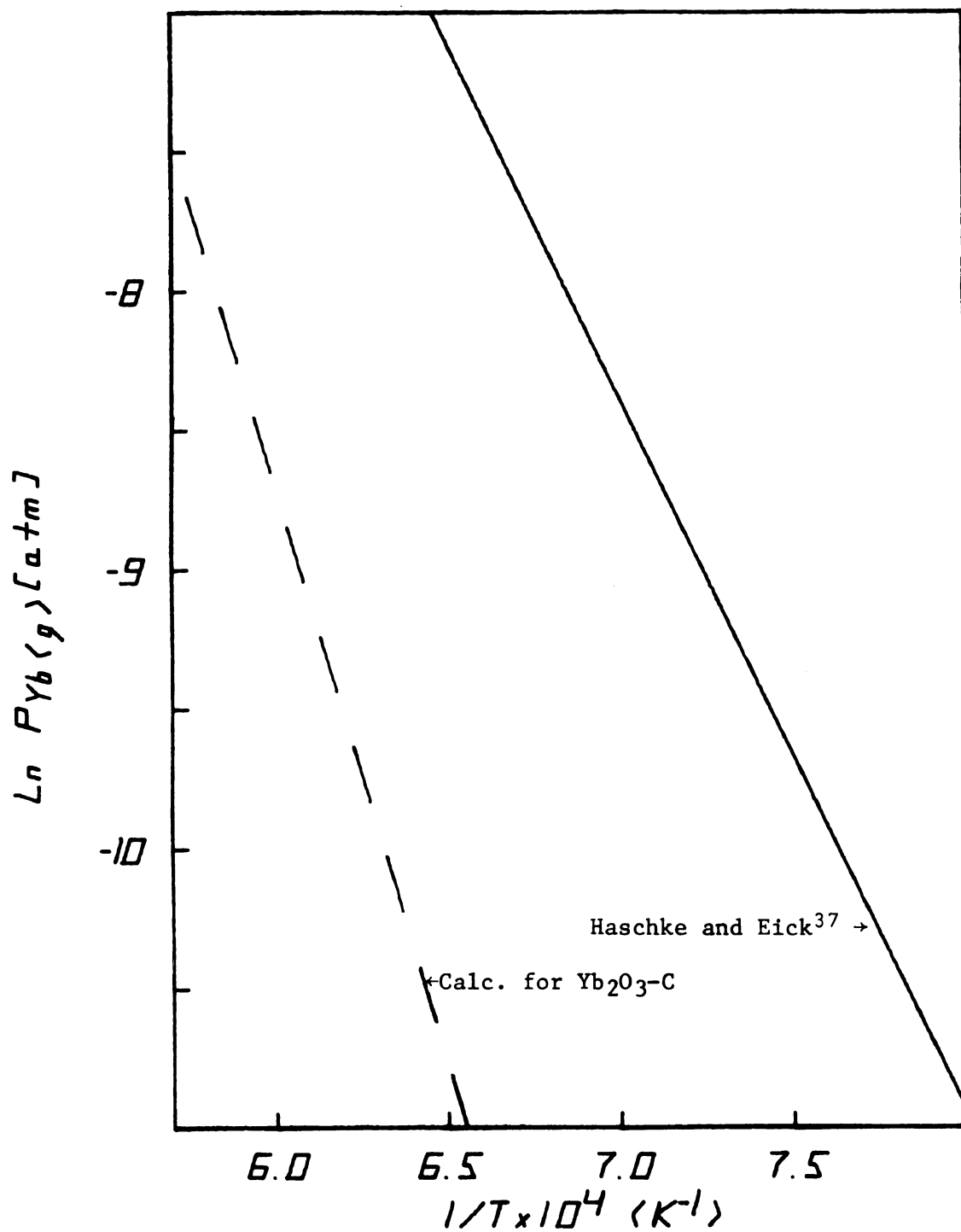


Figure 7. Equilibrium Ytterbium Pressure Reported for YbC_2 and Calculated for $\text{Yb}_2\text{O}_3\text{-C}$

vaporizing mixture is an inert contaminant.

The last class is that of EuC_2 . The results are shown in Figure 8. There is a considerable discrepancy in the reported pressure of EuC_2 , but this calculation cannot unambiguously resolve it, since part of Gebelt's line lies above the upper limit set by the oxide reduction line. There is a large uncertainty in this particular upper limit, because the low temperature calorimetric work on Eu_2O_3 is unsatisfactory and there is a 2.0 eu uncertainty in $S_{298}^\circ(\text{Eu}_2\text{O}_3)$. When better thermodynamic values become available, they may place the pressure of (V-6) for Eu greater than Gebelt's pressure and suggest that his experiments involved an oxide-graphite reaction rather than the dicarbide equilibrium decomposition.

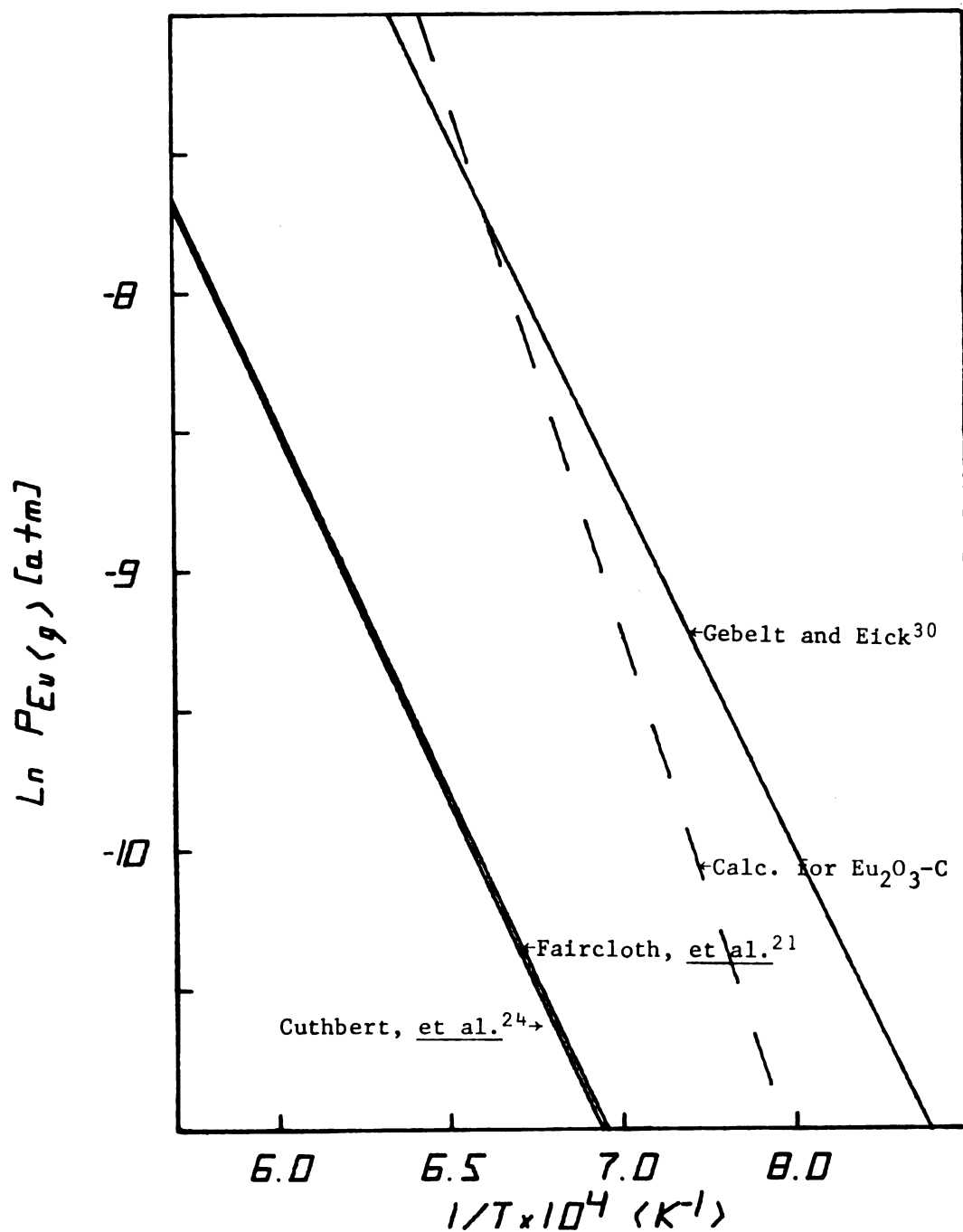


Figure 8. Equilibrium Europium Pressure Reported for EuC_2 and Calculated for Eu_2O_3-C

CHAPTER VI

DISCUSSION

A. Evaluation of Experimental Conditions

1. Sample Handling

Even the stringent procedures adopted for keeping the dicarbide samples free of moisture were not totally successful, as was evidenced by the momentary pressure surge on heating (cf. V,D,5) in experiment 16B. It has been suggested that instead of building glove-boxes in wet rooms, we build dry rooms and let the scientists wear glove suits. Until this procedure becomes practical, it seems necessary to accept and account for inevitable contamination of such extremely hygroscopic materials in the course of handling.

2. The Attainment of Knudsen Conditions

The attainment of most conditions required for Knudsen effusion (cf. III,B,4 and III,B,5) is evidenced by consideration of the trends in the experimental data. The use of the target collection method minimized the effect of the adverse cell length to mean-free-path ratio, the slightly non-ideal orifice, and possible wall losses. The invariance of measured pressures with change in orifice area indicates that there was no serious effect from undersaturation, non-unit vaporization coefficient, or surface diffusion.

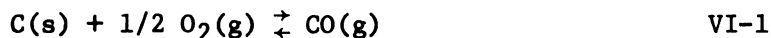
Other investigators have attributed the low enthalpies of vaporization observed in the Sm-C system to diffusion limitations in samarium deficient samples, but the oxide reduction reaction is a

more satisfactory explanation, and no other indications of diffusion limited vaporization were observed. Container-sample interaction was demonstrated to have negligible effect.

In any incongruent vaporization, the two solid phases will exhibit some mutual solubility and thus are not truly at unit activity. As long as this solubility is small and not strongly temperature dependent, it will not affect the consistency of the thermodynamic data. A more subtle effect on the activity of the condensed phases, and on the collection efficiency, is discussed in the next section.

3. An Improved Target Collection Apparatus

In the discussion (section V,F,1) of the oxide reaction it was assumed that all oxygen would eventually be removed from the condensed phase by evolution as CO(g). After the oxygen was gone, the Ln(g) pressure would be that of pure TmC₂. In actuality, it is not possible to remove all the oxygen from the solid because it is impossible to remove all the CO(g) from the system. The CO(g) pressure will be determined by the residual oxygen pressure in the system according to equilibrium (VI-1). Thus it is quite valuable to lower the



residual pressure in the system far beyond the limits set by free path arguments (cf. III,B,5,d).

Since these experiments were completed, the author has designed and constructed a vaporization apparatus capable of a much lower residual pressure. This feat was accomplished through three design features: (1) All glass walls and grease-sealed ground-glass joints were replaced by water-cooled stainless steel walls and OFHC copper gaskets. To permit the metal encasement, the induction coil was placed inside the vacuum chamber. Two frequently opened seals are

fitted with Viton O-rings. (2) The system is pumped by a four-inch diffusion pump charged with Convaless-10, a polyphenyl ether of extremely low vapor pressure and backstreaming characteristics. (3) The chamber is pumped through a straight six inch diameter tube, as short as was practical, to give a high conductance and make full use of the pump speed.

The resulting system operates at 1×10^{-8} torr base pressure, and as low as 3×10^{-8} torr with the sample at 2000° . This is an improvement of two and a half orders of magnitude over the glass system. In the particular case of the dicarbides it is not expected that this lower residual pressure would result in significantly different vapor pressures, but in future studies it will result in increased confidence in the data. Other advantages of the system include the removal of a safety hazard by making the high-voltage induction coil less accessible; more ideal collection efficiency, both due to the lower scattering of the beam and permanent removal of the wide angle effusate by condensation on the chilled, conducting walls; direct mechanical linkage to the target changer; and installation of a thin film monitor in the molecular beam to give immediate indication of orifice clogging, sample depletion, and other similar features.

4. Fluorescence Analysis

X-Ray fluorescence analysis is a very convenient technique for target collection effusion studies. It is non-destructive, sensitive, and requires no preliminary treatment of the sample. The major disadvantage was the tedium of the counting procedures. Recently acquired equipment, including voltage- and current-stabilized power supply, vacuum spectrometer, and high diffraction efficiency graphite analyzing crystal, has reduced analysis time while drastically improving counting statistics. Suggested new methods of standard target preparation, including coulometric deposition of the metals on the targets, should improve the accuracy of the technique

even further.

5. Temperature Measurement

The systematic error in temperature measurement due to the limitations of the pyrometers is quoted to be $\pm 4^\circ$ in the National Bureau of Standards certification. Temperature gradients from the top to the bottom of the crucibles were also around $\pm 4^\circ$. The random error introduced by observer fatigue was estimated to be $\pm 2^\circ$ as determined from a number of successive reading of the standard lamp's temperature. In this study these errors were comparable to the errors in pressure measurement, but with the new target collection and X-ray fluorescence equipment in use, it is anticipated that temperature measurement may be the most significant source of errors in future vaporization studies. More accurate temperature measuring techniques need to be found for further improvement of the target collection technique in this laboratory.

B. The Effects of Oxide Contamination

1. Explanation of the Anomalous Behavior

In view of the known hydrolysis behavior of the dicarbides, it is believed that the anomalous pressures observed over carbon-rich carbide samples results from oxide contamination, with the excess carbon reducing any oxygen bearing species to form CO(g) and Ln(g) . It has been demonstrated that thermodynamically, such a reaction could give a higher lanthanide pressure, and the mechanism also accounts for the higher residual system pressure. The evidence for the presence of CO(g) , although not conclusive, supports this hypothesis.

All reported lower enthalpies of vaporization from high carbon content samarium dicarbide samples have involved experiments conducted with a mass spectrometer. Since several hours are required for complete evolution of

CO(g), these experiments could have been completed before the oxide which caused the high Sm pressure had been removed. Presence of oxygen in near-stoichiometric samples would have been interpreted as presence of excess metal, which causes similar higher pressures. Experimenters would have waited until the pressure stabilized, whether they were using a mass spectrometer or other methods.

Failure to observe an oxide species in X-ray diffraction patterns is not disturbing. First, it would not be present after a vaporization; second, experiment 16C shows that the sesquioxide contamination required is so small that it would be unobservable by this technique; and third, oxide formed by hydrolysis has very poor crystalline structure and would have to be annealed before it could be observed by powder diffraction, even if present in large amounts.

2. The Kinetics Involved

As was shown in section V,F,2, the samarium pressure observed over an oxide-contaminated samarium dicarbide vaporization sample is dependent on the relative rates of the two competing reactions, (V-6) and (V-8). The observation of free metal in quenched preparations of the dicarbide from the oxide indicates that the rate of reduction (V-6) is at least comparable to the rate of formation of the dicarbide. Examination of Figure 5 shows that in some cases it can clearly predominate. Avery, et al. quote results which are in better agreement with the thermodynamics of reaction (V-6) than of (V-2). This observation suggests that the contaminating species is probably one of the oxide carbides which have carbon and oxygen in close proximity in the crystal lattice and not sesquioxide, whose rate of reaction with graphite would be dependent on the low mobilities in the solid phase.

3. The Reaction Trend

The slight variation in lanthanide properties, particularly the volatilities of the dicarbides, has led to a complete reversal of reaction paths in the instance of oxide contamination. The effect of this contamination ranges from nil for YbC_2 , to so great as to be unmistakable for the commonly trivalent metals. Only in the intermediate range of volatility does the oxide contamination seriously interfere in a vaporization study. This conclusion illustrates that interpolation, as well as extrapolation, of the properties of the lanthanide compounds must be done with reservation.

4. Observations Concerning the Preparation of YbC_2 and EuC_2

Since the pressure of Yb over YbC_2 is higher than that over $\text{Yb}_2\text{O}_3\text{-C}$, one would expect that YbC_2 could not be prepared from the oxide and graphite, at least under conditions resembling those in a Knudsen crucible. No report of such a preparation has been found, although most of the other dicarbides have been prepared in this manner⁵. In contrast, a recent report¹²⁷ indicates that EuC_2 can be prepared by graphite reduction of the oxide. This observation suggests that oxide contamination in EuC_2 would have the same effect as that in SmC_2 and TmC_2 .

C. Evaluation of Thermochemical Results

1. Comparison with Previous Work

This work extends and confirms (cf. V,D,6) the vapor pressure values reported for SmC_2 by Faircloth, et al.²¹ and that portion of the work of Cuthbert, et al.²⁴ done by target collection. Both these studies used techniques which were not likely to be affected by oxygen contamination. The pressures reported by Stout, et al.²⁷ agree with the composite line (V-4) to within experimental error

at the higher end of the temperature range and those of Pilato²⁶ agree at the lower end. Avery, et al.²⁵ and Cuthbert's²⁴ mass spectrometric results are both significantly higher and both show the composition dependence noted previously.

2. The Low Temperature Modification of TmC_2

No correction has been made for the enthalpy of the tetragonal-low symmetry transformation of thulium dicarbide.¹⁹ At present it is believed that the "low-symmetry-modification" consists of two phases. Apparently tetragonal TmC_2 disproportionates on cooling, and until some method is developed to prepare the phases in pure form, neither can be characterized satisfactorily. In some respects the behavior of TmC_2 resembles that of UC_2 . Below 1514° UC_2 is unstable with respect to sesquicarbide and graphite, but it is not uncommon to find the non-equilibrium mixture: UC , U_2C_3 , UC_2 , and graphite as the reaction product.¹²⁸ It is possible that one, or both, of the thulium-carbon phases may be oxygen stabilized; Krikorian's¹⁹ results with other heavy lanthanide dicarbides preclude tantalum stabilization.

It is interesting to note that the tetragonal form of LuC_2 has been prepared only from Lu metal samples which contained 2% Ta.¹¹ Krikorian, who used high purity Lu, reports only the "low symmetry modification" of LuC_2 . Since this modification is apparently diphasic, the dicarbide of lutetium may not exist.

It should be understood that the value of $\Delta H_f^{\circ}{}_{298}(\text{TmC}_2(\text{s}))$ herein reported refers specifically to the tetragonal modification.

3. Validity of the Thermodynamic Approximations

The methods used for estimating the thermal functions are generally fairly accurate. If CaC_2 is sufficiently similar to

SmC_2 and TmC_2 to be used as a model, the estimated thermodynamic values should be quite adequate. If CaC_2 is not a suitable model, there is no way to assign an error magnitude to the estimations.

It is characteristic of the methods that the second-law enthalpy is dependent primarily on the experimental data, with a small correction from the thermal parameters, whereas the third law method weights data and thermal functions about equally in determining $\Delta H^\circ_{\text{v}} 298$. This weighting is reflected in the much larger error estimates assigned to the third law values of $\Delta H^\circ_{\text{v}} 298$. Because the experimental data were considered less likely to contain serious systematic error than the thermodynamic function estimates, the second-law $\Delta H^\circ_{\text{v}} 298$ alone was used to calculate $\Delta H^\circ_{\text{f}} 298$, even though use of an average or the third law value alone is more common.

D. The Electronic Ground State of TmC_2

In section V,E,4 it was concluded that the ground state of Tm^{+3} in TmC_2 is non-degenerate. The free-ion ground state is a $^3\text{H}_6$ term, and no other free ion term is low enough to be considered as an alternative ground state in the crystal. Therefore in TmC_2 the crystal field must split the free ion term to a chemically significant degree. At room temperature magnetic susceptibility measurements¹⁷ are consistent with the $^3\text{H}_6$ state, so the splitting must be less than kT at this temperature (200 cm^{-1}), and all the $^3\text{H}_6$ states are thermally populated. However, in the region of 50 K, where antiferromagnetic transitions occur for the other lanthanide dicarbides, kT is only 35 cm^{-1} . The splitting in TmC_2 must be greater than this, so that at this temperature the Tm^{+3} ion is already in a nondegenerate state and there is no driving force for the antiferromagnetic transition. This small crystal field effect is in the range observed for splitting of

f^n configurations¹²⁹, but it is thermodynamically very significant: it results in a change of $\ln P_{Tm}$ over $TmC_2(s)$ of 2.5 units.

E. The Correlation in Vaporization of the Lanthanide and Alkaline Earth Metals and Their Dicarbides

Figure 9 shows Haschke's³⁷ correlation between the enthalpy of vaporization of the lanthanide and alkaline earth dicarbides and the vapor pressure of the pure metals at 1500 K. Those points designated by asterisks have been indicated by Haschke to be in question. The vapor pressures¹²¹ of samarium and thulium at 1500 K and the enthalpies from this study have been included. It is seen that they extend well the linear relationship expected from theoretical considerations¹³⁰.

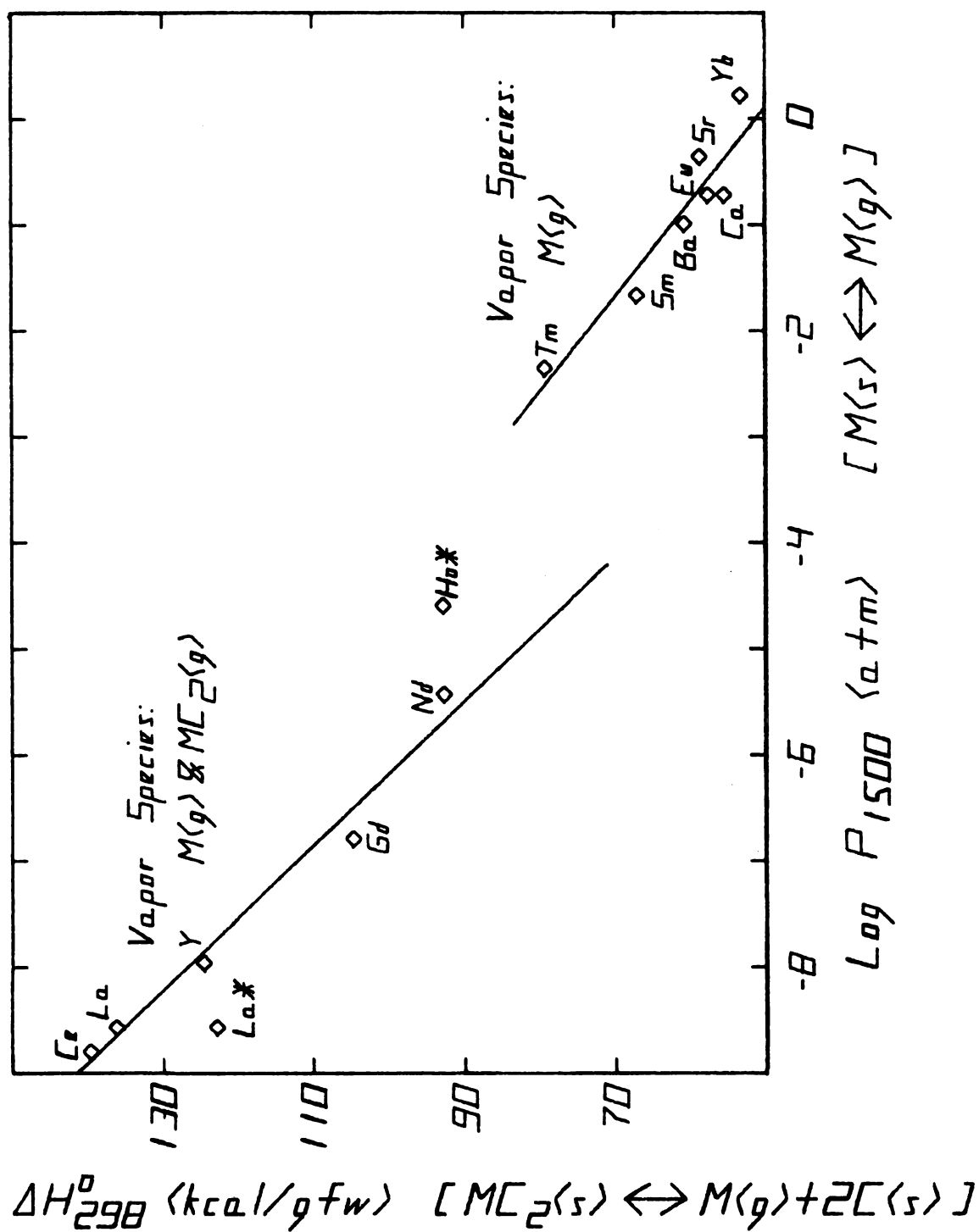


Figure 9. The Correlation of the Metal and Metal Dicarbide Vaporizations

CHAPTER VII

SUGGESTIONS FOR FUTURE RESEARCH

This investigation has indicated several topics which should be investigated to develop a unified body of knowledge concerning the lanthanide dicarbides.

Low temperature heat capacity measurements of tetragonal TmC_2 should be carried out to confirm the standard entropy indicated in this study. Theoretical calculations of the crystal field splittings of the Tm^{+3} ground state in the tetragonal symmetry field would also be valuable, and might indicate other lanthanide compounds in which the crystal field splitting effect could be expected to be chemically significant.

The equilibrium vaporization of EuC_2 should be repeated with special attention paid to the effects of oxygen contamination on the vapor pressure. Alternatively, the calculations performed in section V,F,5 should be repeated as better values become available for the standard entropy of Eu_2O_3 . The vaporization of HoC_2 is also suggested as a significant topic of future study. The effects of oxygen contamination and of carbide vapor species both need to be examined carefully in this system.

Determination of the crystal structures of the orthorhombic and hexagonal phases of the annealed TmC_2 preparations would be an important contribution to the understanding of the transformation to these phases and its thermodynamic implications. Preliminary

experiments indicate that addition of a small amount of iodine to improve the cation mobility may produce samples more suitable for single crystal structural studies.

Experience gained from work with the dicarbides should be used as a basis from which to examine the vaporization behavior of more metal-rich lanthanide carbides.

REFERENCES

REFERENCES

- 1) W. A. Frad, Adv. in Inorg. Chem. and Radiochem., 11, 153 (1968).
- 2) H. Moissan, "The Electric Furnace", trans. by A. T. Mouilpied, Arnold, London, 1904.
- 3) M. v. Stackelberg, Z. physik. Chem., 9B, 437 (1930), and Z. Elektrochem., 37, 542 (1931).
- 4) F. H. Spedding, K. Gschniedner, Jr., and A. H. Daane, J. Amer. Chem. Soc., 80, 4499 (1958).
- 5) R. C. Vickery, R. Sedlacek, and A. Ruben, J. Chem. Soc. 1959, 498.
- 6) A. L. Bowman, N. H. Krikorian, G. P. Arnold, T. C. Wallace, and N. G. Nereson, "Proceedings of the Sixth Rare Earth Research Conference", Gatlinburg, TN, 1967, p 311.
- 7) R. E. Gebelt and H. A. Eick, Inorg. Chem., 3, 335 (1964).
- 8) M. A. Bredig, J. Amer. Ceram. Soc., 43, 493 (1960).
- 9) G. Adachi, H. Kotani, N. Yoshida and J. Shiokawa, J. Less-Common Metals, 22, 517 (1970).
- 10) N. H. Krikorian, J. C. Wallace, and M. G. Bowman, Proceedings, Colloque International Sur les Derives Semimetallique du Centre National de la Rescherche Scientifique de l'Universite de Paris, Orsay, 1965.
- 11) M. Atoji, J. Chem. Phys., 35, 1950 (1961).
- 12) M. Atoji, J. Phys. Soc. Japan, 17, Supp. B-11, 395 (1962); Chem. Abstr., 58, 1978g (1963).
- 13) M. Atoji, Phys. Letters, 22, 21 (1966).
- 14) M. Atoji, ibid., 23, 208 (1966).
- 15) M. Atoji, J. Chem. Phys., 46, 1891 (1967).
- 16) M. Atoji, ibid., 48, 3384 (1968).
- 17) M. Atoji, ibid., 52, 6431 (1970).
- 18) M. Atoji and R. H. Flowers, ibid., 52, 6430 (1970).

- 19) M. C. Krupka, N. H. Krikorian and J. C. Wallace, presented at the Seventh Rare Earth Research Conference, Coronado, California, October 1968; powder pattern courtesy of N. H. Krikorian.
- 20) D. D. Jackson, R. G. Bedford, and G. W. Barton, Jr., AEC Report UCRL-7362-T (1963).
- 21) R. L. Faircloth, R. H. Flowers, and F. C. W. Pummery, J. Inorg. Nucl. Chem., 30, 499 (1968).
- 22) G. Balducci, A. Capalbi, G. De Maria, and M. Guido, J. Chem. Phys., 50, 1969 (1969).
- 23) P. Winchell and N. L. Baldwin, J. Phys. Chem., 71, 4476 (1967).
- 24) J. Cuthbert, R. L. Faircloth, R. H. Flowers, and F. C. W. Pummery, Proc. Brit. Ceram. Soc., 8, 155 (1967).
- 25) D. F. Avery, J. Cuthbert, and C. Silk, Brit. J. Appl. Phys., 18, 1133 (1967).
- 26) P. A. Pilato, Ph. D. Thesis, Michigan State University, East Lansing, MI, 1968.
- 27) N. D. Stout, C. L. Hoenig, and P. C. Nordine, J. Amer. Ceram. Soc., 52, 145 (1969).
- 28) G. M. Kyshtobaeva, E. I. Smagina, and V. S. Kutsev, Zhur. Fiz. Khim., 43, 2400 (1969); Russ. J. Phys. Chem., 43, 1350 (1969).
- 29) G. M. Kyshtobaeva, E. I. Smagina, and V. S. Kutsev, Zhur. Fiz. Khim., 44, 1405 (1970); Russ. J. Phys. Chem., 44, 788 (1970).
- 30) R. E. Gebelt and H. A. Eick, J. Chem. Phys., 44, 2872 (1966).
- 31) D. D. Jackson, G. W. Barton, O. H. Krikorian, and R. S. Newberry, "Proceedings of the Symposium on Thermodynamics of Nuclear Materials", Vienna, 1963, p 529.
- 32) C. L. Hoenig, N. D. Stout, and P. C. Nordine, J. Amer. Ceram. Soc., 50, 385 (1967).
- 33) G. Balducci, A. Capalbi, G. De Maria, and M. Guido, Air Force Materials Laboratory Tech. Report AFML-TR-69-71, 24 pp (1969).
- 34) G. Balducci, A. Capalbi, G. De Maria, and M. Guido, J. Chem. Phys., 51, 2871 (1969).
- 35) G. F. Wakefield, A. H. Daane, and F. H. Spedding, "Proceedings of the Fourth Rare Earth Research Conference, Phoenix, AZ, 1964, p 469.
- 36) G. Balducci, G. De Maria, and M. Guido, J. Chem. Phys., 51, 2876 (1969).
- 37) J. M. Haschke and H. A. Eick, J. Phys. Chem., 72, 1697 (1968).

- 38) W. A. Chupka, J. Berkowitz, C. F. Giese, and M. G. Inghram, J. Phys. Chem., 62, 611 (1958).
- 39) E. E. Filby and L. L. Ames, High Temp. Sci., 3, 41 (1971).
- 40) G. Balducci, A. Capalbi, G. De Maria, and M. Guido, J. Chem. Phys., 43, 2136 (1965).
- 41) G. Balducci, A. Capalbi, G. De Maria, and M. Guido, Air Force Materials Laboratory Tech. Report AFML-TR-67-335, 20 pp, (1967).
- 42) G. De Maria, G. Balducci, A. Capalbi, and M. Guido, Proc. Brit. Ceram. Soc., 8, 127 (1966).
- 43) G. Balducci, A. Capalbi, G. De Maria, and M. Guido, J. Chem. Phys., 48, 5275 (1968).
- 44) E. E. Filby and L. L. Ames, J. Phys. Chem., 75, 848 (1971).
- 45) R. L. Faircloth and R. H. Flowers, U. K. Atomic Energy Authority Report AERE-R-5191, 14 pp (1966).
- 46) F. B. Baker, E. J. Huber, C. E. Holley, Jr., and N. H. Krikorian, J. Chem. Thermo., 3, 77 (1971).
- 47) N. N. Greenwood and A. J. Osborn, J. Chem. Soc., 1961, 1775.
- 48) R. C. Vickery, R. Sedlacek, and A. Ruben, ibid., 1959, 503.
- 49) R. C. Vickery, R. Sedlacek, and A. Ruben, ibid., 1959, 505.
- 50) G. J. Palenik and J. C. Warf, Inorg. Chem., 1, 345 (1962).
- 51) J. S. Anderson, N. J. Clark and I. J. McColm, J. Inorg. Nucl. Chem., 30, 105 (1968).
- 52) K. K. Kelley, Ind. Eng. Chem., 33, 1314 (1941).
- 53) G. E. Moore, ibid., 35, 1292 (1943).
- 54) C. E. Wicks and F. E. Block, "Thermodynamic Properties of 65 Elements - Their Oxides, Halides, Carbides and Nitrides," U. S. Department of the Interior, Bureau of Mines Bulletin 605, U. S. Government Printing Office, Washington, D. C., 1963.
- 55) E. F. Westrum, Jr., Y. Takahashi, and N. D. Stout, J. Phys. Chem., 69, 1520 (1965).
- 56) H. C. Weed and R. J. Morrow, AEC Report UCRL-70245 (1967).
- 57) O. H. Krikorian, AEC Report UCRL-6785 (1962).
- 58) A. L. Bowman, N. H. Krikorian, G. P. Arnold, T. C. Wallace and N. G. Nereson, Acta Cryst., 24B, 1121 (1968).

- 59) M. Atoji and R. C. Medrud, J. Chem. Phys., 31, 332 (1959).
- 60) A. L. Bowman, G. P. Arnold, W. G. Witteman, T. C. Wallace, and N. G. Nereson, Acta Cryst., 21, 670 (1966).
- 61) R. J. L. Andon, J. F. Counsell, J. F. Martin and H. J. Hedger, Trans. Faraday Soc., 60, 1030 (1964).
- 62) J. F. Martin, Proc. Brit. Ceram. Soc., 8, 1 (1967).
- 63) L. S. Levinson, J. Chem. Phys., 38, 2105 (1963).
- 64) A. C. MacLeod and S. W. J. Hopkins, Proc. Brit. Ceram. Soc., 8, 15 (1967).
- 65) A. C. MacLeod, J. Inorg. Nucl. Chem., 31, 715 (1969).
- 66) A. N. Campbell and N. O. Smith, "The Phase Rule," Dover Publications, Inc., New York, NY, 1951.
- 67) G. N. Lewis and M. Randall, "Thermodynamics," Revised by K. S. Pitzer and L. Brewer, McGraw Hill Book Co., Inc., New York, NY, 1961.
- 68) E. D. Cater in "Techniques in Metals Research," Vol. IV, R. A. Rapp, Ed., Wiley-Interscience, Inc., New York, NY, in press.
- 69) M. Knudsen, Ann. Phys., 28, 75 (1909); English translation by L. Venters, Argonne National Laboratory (1958).
- 70) M. Knudsen, ibid., 28, 999 (1909); English translation by K. D. Carlson and E. D. Cater, Argonne National Laboratory (1958).
- 71) J. W. Ward, AEC Report LA-3509 (1966).
- 72) P. Clausen, Physica, 9, 65 (1929).
- 73) R. D. Freeman and J. G. Edwards, "Transmission Probabilities and Recoil Force Correction Factors for Conical Orifices" in "The Characterization of High-Temperature Vapors," J. L. Margrave, Ed., John Wiley and Sons, Inc., New York, NY, 1967, Appendix C.
- 74) K. Motzfeldt, J. Phys. Chem., 59, 139 (1955).
- 75) K. D. Carlson, AEC Report ANL-6156 (1960).
- 76) K. D. Carlson, P. W. Gilles and F. J. Thorn, J. Chem. Phys., 38, 2064 (1963).
- 77) F. Knauer and O. Stern, Z. Physik., 53, 781 (1929).
- 78) J. N. Smith, Jr., J. Chem. Phys., 40, 2520 (1964).
- 79) J. W. Ward, ibid., 49, 5129 (1968).
- 80) G. M. Rosenblatt, P. Lee, and M. B. Dowell, ibid., 45, 3454 (1966).

- 81) G. M. Rosenblatt and P. Lee, J. Chem. Phys., 49, 2995 (1968).
- 82) R. G. Thorn and G. H. Winslow, ibid., 26, 186 (1957).
- 83) G. M. Rosenblatt, J. Phys. Chem., 71, 1327 (1967).
- 84) K. G. Gunther, Z. f. angew. Physik, 9, 550 (1957).
- 85) W. L. Winterbottom and J. P. Hirth, J. Chem. Phys., 57, 784 (1962).
- 86) W. L. Winterbottom, ibid., 49, 106 (1968).
- 87) E. G. Rauh and R. J. Thorn, ibid., 22, 1414 (1954).
- 88) A. Pattoret, J. Drowart and S. Smoes, Trans. Faraday Soc., 65, 98 (1969).
- 89) R. J. Ackermann and E. G. Rauh, J. Phys. Chem., 73, 769 (1969).
- 90) J. W. Ward and R. N. R. Mulford, J. Chem. Phys., 47, 1710 (1967).
- 91) J. W. Ward, ibid., 47, 4030 (1967).
- 92) J. W. Ward, R. N. R. Mulford, and R. L. Bivins, ibid., 47, 1718 (1967).
- 93) J. W. Ward and M. V. Fraser, ibid., 49, 3743 (1968).
- 94) J. M. Haschke, Ph. D. Thesis, Michigan State University, East Lansing, MI, 1969.
- 95) E. Storms, J. High Temp. Sci., 1, 456 (1969).
- 96) R. A. Kent, Ph. D. Thesis, Michigan State University, East Lansing, MI, 1963.
- 97) T. B. Douglas, J. Research, 73A, 451 (1969).
- 98) H. J. Kostkowski and R. D. Lee, "Theory and Methods of Optical Pyrometry," National Bureau of Standards Monograph 41, U. S. Government Printing Office, Washington, D. C., 1962.
- 99) J. L. Margrave, "Physicochemical Measurements at High Temperature," J. Bockris, J. White and J. Mackenzie, Eds., Academic Press, Inc., New York, NY, 1959, Chapter 2.
- 100) W. Parrish, "Advances in X-Ray Diffraction," Centurex Publishing Company, Eindhoven, 1962.
- 101) W. S. Horton, J. Research, 70A, 533 (1966).
- 102) D. Cubicciotti, J. Phys. Chem., 70, 2410 (1966).
- 103) J. R. McCreary and R. J. Thorn, J. Chem. Phys., 50, 3725 (1969).
- 104) R. J. Thorn, ibid., 51, 3582 (1969).

- 105) A. S. Kana'an, J. R. McCreary, D. E. Peterson and R. J. Thorn, High Temp. Sci., 1, 222 (1969).
- 106) J. R. McCreary, S. A. Rassoul, and R. J. Thorn, ibid., 1, 412 (1969).
- 107) R. J. Thorn, J. Chem. Phys., 52, 474 (1970).
- 108) E. R. Plante and R. C. Paule, ibid., 53, 3770 (1970).
- 109) R. C. Petersen, J. H. Markgraf, and S. D. Ross, J. Amer. Chem. Soc., 83, 3819 (1961).
- 110) R. C. Peterson, J. Org. Chem., 29, 3133 (1964).
- 111) J. J. Stezowski, Ph. D. Thesis, Michigan State University, East Lansing, MI, 1968.
- 112) P. G. Hambling, Acta Cryst., 6, 98 (1953).
- 113) O. Lindqvist and F. Wengelin, Ark. Kemi, 28, 179 (1967).
- 114) H. Neff, Siemens Review, 34, 37 (1967).
- 115) J. M. Haschke, R. L. Seiver, and H. A. Eick, AEC Report COO-716-033 (1968).
- 116) J. L. Franklin, J. G. Dillard, H. M. Rosenstock, J. T. Herron, K. Draxl, and F. H. Field, "Ionization Potentials, Appearance Potentials, and Heats of Formation of Gaseous Positive Ions," National Bureau of Standards Report NSRDS-NBS 26, U. S. Government Printing Office, Washington, D. C., 1959.
- 117) R. C. Feber and C. C. Herrick, AEC Report LA-3184 (1965).
- 118) R. C. Feber and C. C. Herrick, J. Chem. Eng. Data, 12, 85 (1967).
- 119) W. M. Latimer, "Oxidation Potentials," 2nd Edition, Prentice Hall, Englewood Cliffs, NJ, 1952, Appendix III.
- 120) E. F. Westrum, Jr., "Advances in Chemistry Series, No. 71, Lanthanide/Actinide Chemistry," R. F. Gould, Ed., American Chemical Society, Washington, D. C., 1967, pp 25-50.
- 121) R. Hultgren, "Supplement to the Selected Values of Thermodynamic Properties of Metals and Alloys," Private Communication ($\Delta H_V^{298} = 49.4 \pm 0.5$ kcal/gfw [Sm] and 55.5 ± 1.0 kcal/gfw [Tm]).
- 122) C. E. Holley, Jr., E. J. Huber, Jr., and F. B. Baker, Prog. Sci. Technol. Rare Earths, 1968, 343.
- 123) A. D. Butherus, R. B. Leonard, G. L. Buchel, and H. A. Eick, Inorg. Chem., 5, 1567 (1966).
- 124) A. D. Butherus and H. A. Eick, J. Amer. Chem. Soc., 90, 1715 (1968).

- 125) J. M. Haschke and H. A. Eick, Inorg. Chem., 9, 851 (1970).
- 126) "JANAF Interim Thermochemical Tables," D. R. Stull, Project Director, Dow Chemical Co., Midland, MI, 1960.
- 127) N. N. Matyushenko and O. P. Svinarenko, Ukr. Fiz. Zh., 13, 1083 (1968); Chem. Abstr., 69, 112961v (1968).
- 128) E. K. Storms, "The Refractory Carbides," Academic Press, New York, NY, 1967.
- 129) F. A. Cotton and G. Wilkinson, "Advanced Inorganic Chemistry," Wiley-Interscience, Inc., New York, NY, 1966, p 1058.
- 130) J. M. Haschke, University of Michigan, personal communication, 1971.

APPENDICES

APPENDIX I: Instructions for Realigning the Guiner Cameras

It is assumed that the operator is familiar with the geometry and basic operation of the Guiner camera and with good X-ray safety techniques.

CAUTION: During the alignment process the X-ray generator will frequently be energized without the usual shielding material in place. The lead apron should be worn at all times. When checking with the fluorescent screen, a lead-glass plate should be placed over the box. For making adjustments with the beam on, wear the lead gloves.

A. Preliminary Setup

- (1) Remove and identify each piece of the camera as shown in Figure A-1.

If the crystal is not to be changed, do not take apart the monochromator assembly; omit part B.

- (2) If X-ray tube has been moved, optimize as follows. If only the box has been moved or if the other camera has already been realigned, omit (a) and (b).

- (a) Move box to center of its motion (three bolts on bottom) with respect to forward-back, sideways, and twist motions.

- (b) With Azaroff beam tunnel in place, glass plate over top of box, lead apron on, and a fluorescent screen in front of window in box, turn the generator on to 25 KV, 5 mA. Turn off room lights and open shutter. Slide the X-ray tube back and forth in the dovetail until the image in the fluorescent screen is a full circle of maximum intensity. Lock the tube in position with the Allen head set screw.

- (c) Put the main base plate in the box and mount the monochromator vernier base plate on it with the two long screws, again with it in the center of its motion.
 - (d) Move the box sideways until the pin on the vernier plate is 9 cm from the tube anode (center of the tube housing), without disturbing the forward-back position; or, if (b) was omitted, move box forward or back at this time to meet the conditions of (b). (Note: This pin marks the exact center of the monochromator crystal.)
- (3) Remove the vernier plate. Using a small level adjust the three leveling screws until the main base plate is parallel to the top face of the tube mount-shutter assembly. Turning all three screws the same amount to maintain this level, raise or lower the main base plate to 1-1/8" below the center of the window in the box. Recheck the level, then lock the leveling screws.
- (4) Plotting The Beam Path - With the beam on (25KV, 5mA) use the fluorescent screen to find the center of the beam at several distances from the tube (8-25 cm) and mark it on the main base plate. Scribe a line through these points.
- (5) Replace the vernier plate so that:
- (a) The pin lies exactly on the line just scribed.
 - (b) The pin is 9.0 cm from the anode.
 - (c) Within these limitations, the plate is as far counter-clockwise as possible (for the right camera; for the left, clockwise).

B. Replacing the Monochromator Crystal

Unless the crystal has to be changed, do not disassemble the monochromator assembly. Omit this section.

- (1) Remove the knurled bolt and the monochromator slit from the assembly. Carefully remove the four spring-loaded bolts from the back of the monochromator assembly and lift off the back and crystal.
- (2) Remove the crystal from the back by soaking in petroleum ether or other solvent suitable for rubber cement (be patient).
- (3) Clean the monochromator housing. Lay a thin bead of rubber cement along both supporting edges of the back of the monochromator.
- (4) Carefully rub both sides of the crystal with HB pencil and then clean off.
- (5) With curvatures matching lay the crystal on the assembly back so that it touches both alignment pins and is centered lengthwise. Press lightly to contact the cement well.

CARE-BREAKAGES ARE COSTLY

NOTE-If crystal breaks it is still possible to use the bits.

- (6) Lower the assembly front over the alignment pins, carefully invert the assembly, and put in the spring-loaded bolts, tightening evenly and carefully to just finger-tight. Replace the slit and knurled bolt - it is impossible to tell which side is up at this time.

C. Aligning the Monochromator

- (1) Mount the monochromator on its base plate and put the assembly over the pin on the vernier plate, with the adjustment bar between the supports for the vernier screw and spring.

- (2) Place the fluorescent screen about 3 cm from the assembly so that the primary beam will just show in the back edge of the screen. Put on the cover glass and turn off the room lights.
- (3) With the generator at 30 KV, 12 mA, use a screwdriver on the adjustment bar to rotate the monochromator back and forth. At the right angles both $K\alpha$ and $K\beta$ diffracted beams will appear near the front of the screen as bands about 1 cm wide. The $K\alpha$ reflection can be distinguished because it is much brighter and occurs at higher angle, i. e., adjustment bar further from the tube housing. Adjust roughly to maximum intensity for $K\alpha$.
- (4) Slide the fluorescent screen back away from the monochromator until the diffracted image appears as a sharp line. This will occur with the screen either 5 cm or 14 cm from the monochromator. If the focus is at 5 cm, the monochromator is upside down. Remove the monochromator, take out the knurled bolt and monochromator slit, take off the base plate and put it on the other side. Replace the slit (fully open) and bolt. Repeat sections C-(1), -(2) and -(3).
- (5) Put adjustment screw in vernier plate and tighten until it just touches adjustment bar. Remove the monochromator and insert the spring-loaded pin. (It may be necessary to loosen the screw; count the turns and retighten it after monochromator is back in.) Replace the monochromator.
- (6) With the X-rays on again, $K\alpha$ should still appear in the fluorescent screen, or should appear with slight adjustment. Tighten the adjustment screw until the reflection just disappears, then loosen it to the other extinction. This should require about a 360° rotation of the adjustment screw.

- (a) For $K\bar{\alpha}$ radiation, tighten the screw 180° from extinction.
(For routine identification and examination for presence of minor phases.)
- (b) For $K\alpha_1$ radiation, tighten the screw 240° from extinction.
(Around 50% as intense but sharper lines with more precise wavelength; for accurate lattice determination.)

D. Aligning the Cassette Mount

- (1) Install the secondary beam base plate with its notch around the pin on the underside of the vernier plate. Put in the two medium-length bolts loosely.
- (2) With X-rays on move this plate until the pin on it (marking the center of the sample) is in the exact center of the diffracted beam. Tighten the bolts temporarily.
- (3) Place a celluloid millimeter scale firmly along the long front edge of this plate with masking tape, so that it can be moved parallel to the beam without disturbing the adjustment just made.
- (4) Place the triangular cassette support plate over the pin on the secondary beam plate and insert the short bolt loosely. Mount the cassette on it with the leather strap swung back out of the way and the primary beam shutter open. Rotate the triangular plate fully toward you and place the fluorescent screen just behind it.
- (5) With X-rays on, rotate the plate slowly away. Image will disappear, then reappear in the primary beam opening. Rotate plate back and forth to center image in this opening.
- (6) Turn off X-rays, carefully remove cassette, and tighten bolt. Replace cassette.

- (7) Check this alignment by closing the primary beam shutter with the beam on. The image should disappear when the shutter is about halfway closed. If it is not fairly close to halfway, repeat D-(5) and -(6).

E. Focussing

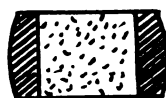
- (1) Loosen the bolts holding the secondary beam base plate and move it against the millimeter scale all the way toward the tube.
- (2) Load the cassette with a short piece of film (3-5 cm) in black paper, so that the film is in the path of the primary beam. Primary beam shutter should be open.
- (3) Expose the film for one second at 18 KV, 1 mA. (May have to be varied slightly for best results.)
- (4) Develop as usual, scrubbing off the back emulsion, and label with the scale reading at the outside edge of the secondary beam plate.
- (5) Move the secondary beam plate out one millimeter.
- (6) Repeat steps (2) through (5) until the secondary beam plate is at the other limit of its motion. (Usually 5-10 exposures)
- (7) Place the film strips on a light box in order and examine with a hand lens. For $K\alpha_1$, there should be a single line which goes through a maximum sharpness. Set the secondary beam plate at the optimum distance and tighten securely. For $K\alpha$, there should be two lines, separated by about 0.1 mm, with the line furthest from the diffraction area ($K\alpha_2$) lower in intensity by about a factor of four. These should be optimized with respect to both sharpness and resolution, and the secondary beam plate set as above. If the intensity ratio is too far

from 1:4, the adjustment screw should be rotated clockwise slightly to enhance $K\alpha_1$ or counterclockwise to enhance $K\alpha_2$ and all steps from D-(1) must be repeated.

F. Slits and Sample Holder

- (1) Position the sample holder 5.25 mm from the flat face of the cassette using the specially machined spacing insert that fits in the sample holder. It should be centered in its travel perpendicular to the beam. Remove and store the spacing insert.
- (2) Install the entrance slit assembly with the slits fully open and the side slits loose. With X-rays on, (25 KV, 5 mA) close the side slits until the bright green portion of the image of the primary beam in the fluorescent screen (the beam not diffracted by the monochromator) just disappears on each side (see below).

Slits fully open:



Slits properly adjusted:

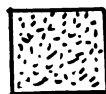
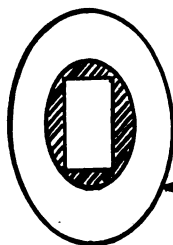


Image of crystal
in direct beam

- (3) Remove the entire assembly on its base plate and place it on a table. Adjust the top and bottom entrance slits until they are just below and above the top and bottom edges, respectively, of the opening in the crystal holder. Measuring with a vernier caliper from the base plate is a convenient method.
- (4) With a strong light coming through the crystal and sample holder, and an empty steel target in the holder, sight through the primary beam opening of the cassette and close the sample slits until none of the steel disc will be in the beam path, as shown on the next page.



Steel sample disc (viewed at an angle and thus foreshortened to an ellipse)

- (5) Replace the unit in the box and plug in the sample motor.
- (6) Put in the stray radiation shield.

G. Checkout

- (1) Take a one hour exposure of KCl (35 KV, 18 mA). Read the film and calculate a correction factor from the tables in the Guinier manual. (Note separate tables for $K\bar{\alpha}$ and $K\alpha_1$.) For our cameras the correction factor is usually 0.985 ± 0.010 . For $K\bar{\alpha}$, there will be a slight decrease in $S_{\text{calc}}/S_{\text{obs}}$ with increasing S_{obs} ; for $K\alpha_1$ this trend should not be present.
- (2) With an empty steel disc mounted, take a 24 hour exposure (35 KV, 18 mA). If no metal parts are struck by the beam, a diffuse film with no sharp lines should be obtained. Excessive darkening at low angles can be reduced somewhat by moving the monochromator slit in about 3/4 of the way, with no serious loss in intensity.

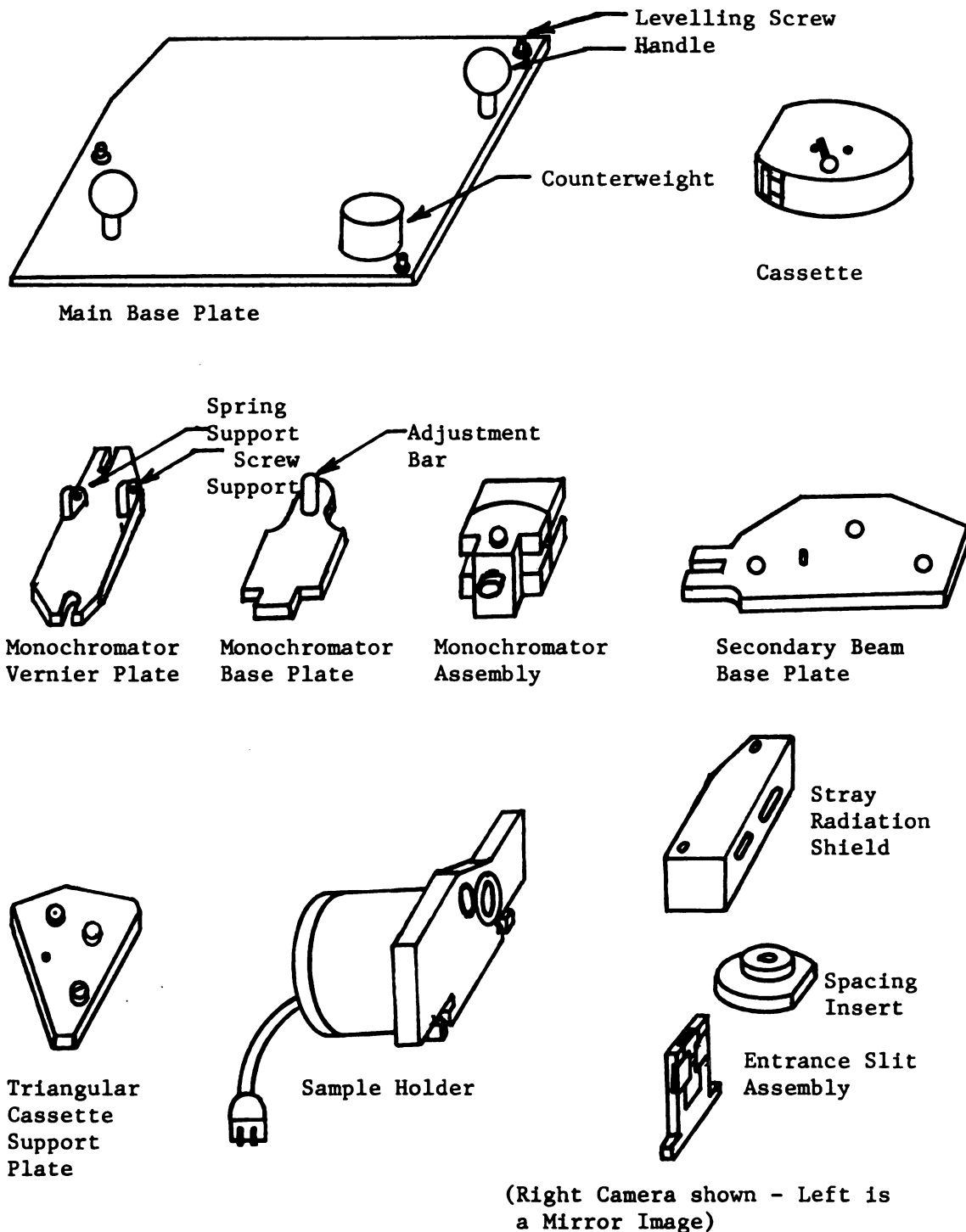


Figure A-1. Parts of the Guinier Camera

APPENDIX II: The Observed X-Ray Powder Diffraction Pattern of the
Black Form of TmC_2

Relative Intensity*	$\sin^2\phi$	d-value (Å)	Assignment		
			Orth.	Hexagonal	Other
2	0.00312	13.79	001		
5	0.01278	6.813	002		
2	0.01582	6.124	020		
3	0.01862	5.645	021		
3	0.02825	4.583	022		
6	0.04443	3.654	100		
2	0.04713	3.548	101		
5	0.05024	3.436	111		
4	0.05147	3.395	004		
4	0.05263	3.357			Graphite 00·2
2	0.05541	3.272	014		
4	0.05986	3.148	120		
5	0.06188	3.096	040		
6	0.06239	3.084			Tetragonal TmC_2 101
5	0.06514	3.018			Tetragonal TmC_2 002
10	0.06703	2.975	024		
5	0.07469	2.818	042		
7	0.07618	2.791		00·6	
7	0.07866	2.746		10·1	
4	0.07923	2.736	130		
2	0.08064	2.712	005		
5	0.08281	2.677	131		

APPENDIX II: (continued)

8	0.08600	2.627		10·2	
8	0.08872	2.586			TaC 111
3	0.09064	2.558			Tetragonal TmC_2 110
5	0.09570	2.490	104		
6	0.09871	2.452		10·3	
2	0.10108	2.423	051		
2	0.10757	2.348	133		
5	0.11175	2.304		10·4	
3	0.11604	2.261	006		
4	0.12075	2.217			TaC 200
3	0.12776	2.155	115		
4	0.13034	2.134		10·5	
5	0.13154	2.124	026		
4	0.14230	2.040	151		
4	0.14843	1.999	054		
4	0.15219	1.974	062		
4	0.15680	1.945	144		
8	0.16330	1.906	017		
4	0.16554	1.893	116		
4	0.16847	1.877	153		
3	0.17342	1.850	126		
6	0.17629	1.835	200		
7	0.18146	1.808		10·7	

*Visually estimated

APPENDIX III: Values of Δf_{ef} For Reactions (V-1) and (V-2)

T, K	Δf_{ef} , vaporization of SmC_2	Δf_{ef} , vaporization of TmC_2 , with no magnetic contribution	Δf_{ef} , vaporization of TmC_2 , with magnetic contribution
1600	-18.69	-22.80	-17.70
1700	-18.55	-22.53	-17.43
1800	-18.43	-22.29	-17.19
1900	-18.30	-22.07	-16.97
2000	-18.18	-21.84	-16.74
2100	-18.08	-21.65	-16.55
2200		-21.46	-16.36

APPENDIX IV: Equilibrium Pressure and Third Law Enthalpy Data

APPENDIX IVA: Samarium Dicarbide

T, K	- ln P (atm)	$\Delta H_v^{\circ}{}_{298}$ (kcal/gfw)
1656	10.9705	66.92
1744	9.9728	66.81
1838	8.9103	66.32
1925	7.9331	65.52
1908	8.2058	66.01
1857	8.7272	66.28
1795	9.4522	66.79
1725	10.2512	67.08
1717	10.1279	66.37
1782	9.4932	66.49
1865	8.6788	66.37
1988	7.5816	66.13
1914	8.2037	66.20
1851	8.7833	66.29
1767	9.6885	66.65
1631	11.2951	67.02
1916	8.3315	66.75
1882	8.7037	67.03
1804	9.3770	66.84
1770	9.8868	67.45
1690	10.5158	66.69
1792	9.1908	65.76
1853	8.7012	66.05

APPENDIX IVA: (continued)

1935	8.0409	66.25
1899	8.5660	67.08
1827	9.2338	67.12
1765	9.8334	67.08
1696	10.5503	67.03
1708	10.2832	66.57
1799	9.3475	66.56
1717	10.0864	66.23
1821	8.9226	65.79
1872	8.4577	65.78
1945	8.0568	66.63
1896	8.4747	66.63
1860	8.7999	66.65
1772	9.6636	66.73
1720	10.2239	66.81
1914	8.1769	66.09
1861	8.7485	66.50
1829	9.0593	66.55
1788	9.4468	66.53
1726	10.0743	66.51
1772	9.5719	66.41
1834	9.0691	66.76
1944	8.1018	66.77
1986	7.7522	66.74
1879	8.6182	66.61
1797	9.3334	66.44

APPENDIX IVA: (continued)

1712	10.3783	67.04
2009	7.5073	66.48
1967	7.9339	66.85
1893	8.1988	65.50
1745	9.7553	66.10
1788	9.5776	67.00
1896	8.5792	67.03
1975	7.8348	66.72
2026	7.3175	66.24
2053	7.0919	66.15
2025	7.2765	66.05
1935	8.0805	66.40
1829	9.0498	66.52

APPENDIX IVB: Thulium Dicarbide

T, K	- ln P (atm)	$\Delta H_{f, 298}^{\circ}$ (kcal/gfw)	
		with magnetic contribution	without magnetic contribution
1664	12.5053	70.51	79.00
1748	11.3329	69.63	78.55
1808	10.6263	69.22	78.44
1886	9.7908	68.74	78.36
1926	9.3703	68.42	78.24
1876	9.9268	68.92	78.49
1832	10.3218	68.93	78.27

APPENDIX IVB: (continued)

1761	11.2421	69.178	78.176
1688	11.8857	69.35	77.96
1751	11.1825	69.22	78.15
1798	10.6897	69.11	78.28
1860	10.0639	68.91	78.40
1913	9.6322	69.01	78.76
1950	9.2739	68.79	78.74
1879	9.8816	68.85	78.44
1840	10.3087	69.15	78.53
1948	9.2276	68.55	78.49
2006	8.8139	68.70	78.93
2066	8.1593	67.82	78.35
2125	7.8580	68.24	79.08
2080	8.2360	68.54	79.14
1968	9.1079	68.70	78.74
1792	10.9415	69.80	78.94
1758	11.2581	69.73	78.69
1712	11.9031	70.29	79.02
1676	12.2289	70.05	78.60
1907	9.6658	68.94	78.67
2013	8.6356	68.20	78.46
1871	9.9698	68.92	78.46
1806	10.7067	69.44	78.65
1745	11.3927	69.73	78.63
1824	10.5499	69.49	78.79
1899	9.7424	68.98	78.66
1992	8.8670	68.49	78.65

APPENDIX IVB: (continued)

2035	8.4437	68.08	78.45
2127	7.8916	68.44	79.29
2063	8.2034	67.91	78.43
2012	8.6931	68.40	78.66
1875	9.9856	69.11	78.67
1698	11.9632	69.98	78.64
1724	11.7668	70.26	79.06
1784	11.0494	69.91	79.00
1856	10.1470	69.09	78.55
1809	10.7607	69.74	78.97
1770	11.1951	69.93	78.96
1710	11.9991	70.54	79.26

MICHIGAN STATE UNIVERSITY LIBRARIES



3 1293 03174 5700